OPO OPHTHALMIC & PHYSIOLOGICAL OPTICS
THE JOURNAL OF THE COLLEGE OF OPTOMETRISTS

Ophthalmic & Physiological Optics ISSN 0275-5408

INVITED REVIEW

The fundus photo has met its match: optical coherence tomography and adaptive optics ophthalmoscopy are here to stay

Jessica I. W. Morgan

Department of Ophthalmology, Scheie Eye Institute, Perelman School of Medicine, University of Pennsylvania, Philadelphia, USA

Citation information: Morgan JIW. The fundus photo has met its match: optical coherence tomography and adaptive optics ophthalmoscopy are here to stay. *Ophthalmic Physiol Opt* 2016; 36: 218–239. doi: 10.1111/opo.12289

Keywords: adaptive optics ophthalmoscopy, angiography, optical coherence tomography, photoreceptors, retinal and choroidal vasculature, scanning laser ophthalmoscopy

Correspondence: Jessica I. W. Morgan
E-mail: jwmorgan@mail.med.upenn.edu

Received: 13 November 2015; Accepted: 20 January 2016

Abstract

Purpose: Over the past 25 years, optical coherence tomography (OCT) and adaptive optics (AO) ophthalmoscopy have revolutionised our ability to non-invasively observe the living retina. The purpose of this review is to highlight the techniques and human clinical applications of recent advances in OCT and adaptive optics scanning laser/light ophthalmoscopy (AOSLO) ophthalmic imaging.
Recent findings: Optical coherence tomography retinal and optic nerve head (ONH) imaging technology allows high resolution in the axial direction resulting in cross-sectional visualisation of retinal and ONH lamination. Complementary AO ophthalmoscopy gives high resolution in the transverse direction resulting in en face visualisation of retinal cell mosaics. Innovative detection schemes applied to OCT and AOSLO technologies (such as spectral domain OCT, OCT angiography, confocal and non-confocal AOSLO, fluorescence, and AO-OCT) have enabled high contrast between retinal and ONH structures in three dimensions and have allowed *in vivo* retinal imaging to approach that of histological quality. In addition, both OCT and AOSLO have shown the capability to detect retinal reflectance changes in response to visual stimuli, paving the way for future studies to investigate objective biomarkers of visual function at the cellular level. Increasingly, these imaging techniques are being applied to clinical studies of the normal and diseased visual system.
Summary: Optical coherence tomography and AOSLO technologies are capable of elucidating the structure and function of the retina and ONH noninvasively with unprecedented resolution and contrast. The techniques have proven their worth in both basic science and clinical applications and each will continue to be utilised in future studies for many years to come.

Introduction

Practically overnight, Herman von Helmholtz's invention of the ophthalmoscope in 1851 radically changed the field of ophthalmology by allowing non-invasive observation of retinal and optic nerve head (ONH) pathophysiology. Jackman and Webster used this concept, along with the newly emerging field of photography, to record and publish the first images of the fundus in the living human eye in 1886.[1] In the years that followed, fundus photography to record patient's ophthalmoscopic findings naturally proceeded and became an important procedure for the diagnosis and assessment of retinal and ONH disease. For almost a century, fundus photography using flood illuminated reflectance imaging was the only method available for acquiring pictures of the retina and ONH. Then, by both careful design and some luck,[2] the technique of fluorescein angiography for investigating retinal circulation was developed and published by Novotny and Alvis in 1961.[3] The clinical utility of this technique was quickly realised and fluorescein angiography joined fundus photography as a standard care ophthalmic procedure. Even today, 54 years later, fluorescein angiography remains the gold standard for assessing the

involvement of retinal and choroidal blood vessels in ophthalmic disease.

In the technological age in which we currently live, technology and its applications continue to advance at exponential rates, and the field of retinal imaging is no exception. Despite fundus photography and fluorescein angiography remaining staples in ophthalmic clinical care, investigators are aware of the limitations provided by these techniques. In particular, both fundus photography and fluorescein angiography provide only a macroscopic view of the retina and ONH and both have limited capabilities for examining the three dimensional structure of the tissue. Indeed, the retina and ONH are three-dimensional structures, and microscopic visualisation of its features depends on the axial and transverse resolution inherent to the imaging system, along with the contrast available to distinguish neighbouring features from each other. With this in mind, several other retinal imaging techniques have emerged in recent years, many with the goal of investigating the structure and function of the retina with microscopic detail. To date, at least two of these techniques, both described in the 1990's, again possess the power to fundamentally change the clinical applications of retinal imaging as we previously knew them.

The first of these techniques is optical coherence tomography (OCT). OCT is based on low coherence interferometry, which had been previously used to measure axial distances in the eye.[4,5] Time domain OCT (TD-OCT), introduced in 1991 by Huang *et al.*,[6] measures the interference signal generated between reflections from a reference arm and a sample arm of an interferometer, where the eye is the sample. In its first application, the TD-OCT system recorded the interference signal between reflections from the reference and the sample backscattering positions, and then translated the reference arm in depth to create a longitudinal scan (A-scan). Thus, the signal observed in an A-scan results from interference between the light reflected from the reference arm and the light backscattered from features in the retina located at different depths. By collecting a series of laterally translated A-scans, a cross-sectional retinal image is created (B-scan). The axial resolution of OCT depends only on the coherence length of the imaging source, which is directly proportional to the square of the central wavelength and inversely proportional to the bandwidth of the imaging source.[4,7] Therefore increasing the bandwidth of the source (i.e. decreasing the coherence length) will increase the axial resolution of the system, while increasing the central wavelength of the source will decrease the axial resolution. The low coherence sources used in OCT imaging result in high axial resolution in the cross sectional images; commercially available OCTs currently boast axial resolutions of 5 μm or better (examples include: RTVue-XR Avanti http://www.optovue.com/products/avanti/, Cirrus HD-OCT http://www.zeiss.com/meditec/en_us/products—solutions/ophthalmology-optometry/glaucoma/diagnostics/optical-coherence-thomography/oct-optical-coherence-tomography/cirrus-hd-oct.html, Envisu C-Class http://www.leica-microsystems.com/products/optical-coherence-tomography-oct/details/product/envisu-c-class/). Though TD-OCT was immediately understood to be clinical useful, the technique was limited by the acquisition time required to translate the reference arm of the system. Spectral domain OCT[8,9] (SD-OCT) overcame this limitation by keeping the reference arm static and using a spectrometer to detect the OCT signal. SD-OCT is mathematically related to TD-OCT by the Fourier transform. This SD-OCT approach resulted in vastly increased imaging speeds as well as higher sensitivity when compared with TD-OCT.[10–12] The result is that SD-OCT has made possible the routine acquisition of volume scans over the retina. A third detection scheme for OCT is swept source OCT (SS-OCT), in which a tuneable light source is rapidly swept through a broad bandwidth while the path lengths of the reference and sample arms of the interferometer are held constant.[13,14] Like SD-OCT, SS-OCT operates in the Fourier space and has the equivalent signal to noise ratio and sensitivity advantage of SD-OCT.[13] The value of the information contained within each OCT retinal and ONH image, combined with the ease with which these images now are obtained has truly revolutionised standard ophthalmic care.

The second of the current techniques to fundamentally change retinal imaging came with the invention of adaptive optics (AO). Adaptive optics for ophthalmic applications was first described in 1997.[15] This technique involves measuring and then correcting the ocular optical aberrations, typically by using a wavefront sensor and wavefront corrector, such as a Shack–Hartmann wavefront sensor paired with a deformable mirror. By changing the shape of the wavefront to compensate for the eye's optical aberrations, AO enables imaging with transverse resolution that approaches the fundamental resolution limit (diffraction) through the dilated pupil. It is worth noting that AO on its own is not a retinal imaging modality. Rather, it is a tool used for correcting the aberrations of an optical system (in this case the eye) that is then incorporated into retinal imaging systems such as flood illumination fundus photography,[15] scanning laser/light ophthalmoscopy (SLO),[16] and OCT.[17] While ground-breaking work has been accomplished using both AO flood illumination and AO-OCT, the AO portion of the current review focuses primarily on adaptive optics scanning laser/light ophthalmoscopy (AOSLO) because of its high impact applications and its increased use in clinical research.

Optical coherence tomography and AOSLO embody powerful and complementary techniques, and each has fundamentally changed retinal and ONH imaging by allowing scientists the ability to routinely visualise retinal and ONH structures with cellular resolution in either cross-section or

en face views respectively. Further, combining standard clinical imaging with results from these complementary imaging techniques provides a more complete understanding of the anatomy under investigation (*Figure 1*). This in turn has opened new avenues for clinical applications of retinal and ONH imaging as scientists and clinicians have begun to investigate the structural and functional health of normal and pathological retina and ONH *in vivo* with resolution approaching that of histology. Numerous reviews of these two distinct technologies are available[18–25] that include ample figures and references showcasing normal and diseased anatomy observed through OCT and AOSLO imaging. Therefore the present review does not provide extensive figures of disease cases; rather the purpose of the present review is to highlight recent technical advances in both OCT and AOSLO human imaging, with a focus on current and future clinical applications for these technologies.

Optical coherence tomography structural imaging beyond the spectral domain

Over a relatively short period of time, SD-OCT systems have become an integral part of standard ophthalmic care. In today's ophthalmology clinics, SD-OCTs are used daily to characterise and document the involvement of retinal and ONH layers in ocular complications and retinal and ONH disease. For a review of the basic principles involved with SD-OCT, see van Velthoven *et al.*[20] The wide-spread availability of SD-OCT devices has led to new innovative methodologies for elucidating retinal structures beyond what is routinely acquired in clinical settings. In addition, the fast acquisition speed of SD-OCT makes possible the volumetric imaging protocols required for the advanced three-dimensional imaging applications described below.

Optical coherence tomography angiography

Recent developments in OCT imaging have included non-invasive visualisation of blood vessel perfusion, without the insertion of intravenous dyes. These techniques include Doppler OCT and OCT angiography, and they are accomplished through the differential analysis of multiple OCT scans. The basic principle of Doppler OCT and OCT angiography involves determining the change in backscattering between consecutive A-scans and B-scans, respectively, and then attributing the differences entirely to the

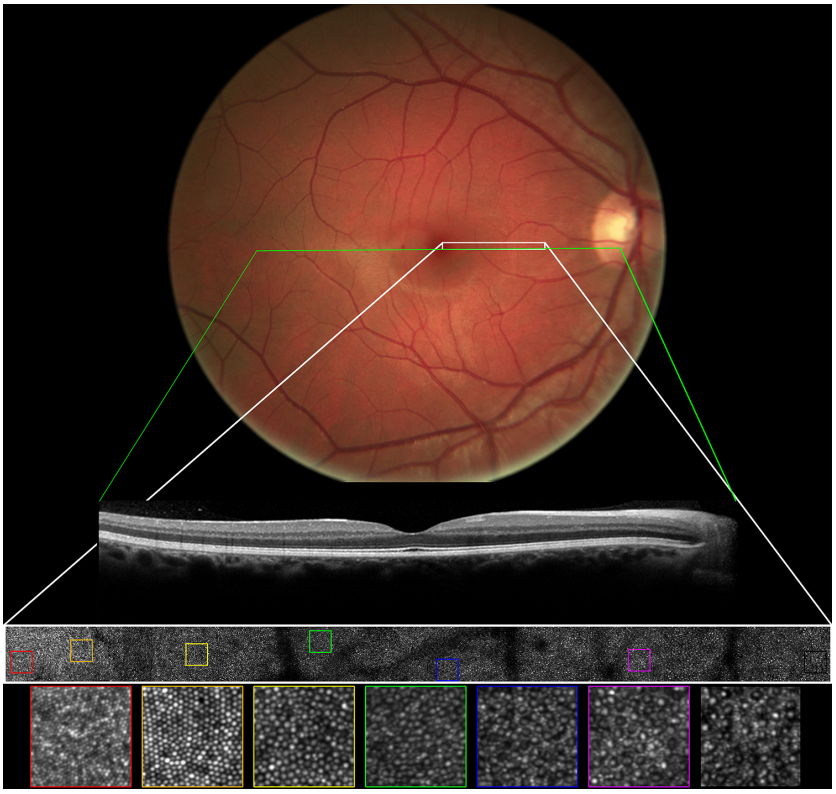

Figure 1. Comparison of a conventional fundus photograph, an SD-OCT cross sectional image obtained along the green line overlaid on the fundus photograph, and a montage of confocal AOSLO images acquired within the white box overlaid on the fundus image in the right eye of a 31 year old normal male. Coloured box outlines on the AOSLO montage show areas of the photoreceptor mosaic in higher magnification below.

flow of erythrocytes through retinal and choroidal blood vessels. This has been accomplished through a number of methods, including Doppler OCT,[26–28] dual beam-scanning OCT,[29,30] phase-variance OCT,[31–33] and split spectrum amplitude decorrelation.[34] Regardless of which method is used to calculate the differences between scans, OCT angiography techniques rely on the assumption that all differences arise from blood flow and that the backscattering associated with retinal and ONH tissue outside of the blood vessels remains static. The split-spectrum amplitude-decorrelation angiography algorithm introduced by Jia *et al.*[34] is most frequently used in OCT angiography studies to date.

By determining the difference between consecutive B-scans at the same location over the entire en face area imaged, OCT angiography allows a volumetric rendering of blood vessels.[35] Further, by segmenting layers of the retina, blood vessels corresponding to specific retinal depths can be projected onto a two-dimensional image. For example, the superficial vascular plexus located in the nerve fibre and ganglion cell layers can be differentiated from the deep vascular plexus located in the inner nuclear layer, simply by segmenting the OCT angiography volume scans at these levels and viewing the en face projections from these two layers separately. The choroidal vascular network, in particular the choriocapillaris, also becomes visible using this same technique (*Figure 2*). Some studies have also imaged Sattler and Haller's layers in the choroid,[36] and it is reasonable to expect that future studies of OCT angiography will allow increased visualisation of these layers by adapting techniques, such as using longer wavelength sources, to allow deeper penetration into the retinal tissue.

Care must be used in interpreting OCT angiography images, first because the images are subject to several artefacts, and second because the imaging detection scheme utilised imposes theoretical limits on the visualisation of vascular perfusion. As an example, fixational eye motion can be a huge problem for OCT angiography, because the algorithm for angiography images assumes that all differences are caused by blood flow. Thus, eye motion results in image artefacts such as white lines, quilting, skewing, stretching, distortions, and even doubling of vessels.[37] In addition, OCT angiography images are subject to projection artefacts, where the vessels from one retinal layer also appear in more posterior layer segmentations. This occurs because as the amount of light reflected from a particular layer of blood vessels changes, so does the amount of light transmitted through the vessels. This causes a change in the amount of incident imaging light on more posterior layers, and thus results in a measurable difference in reflection coming from posterior layers in the same shape as the more anterior blood vessels.[37] Software algorithms have been implemented to minimise projection artefacts,[38] though, care in image interpretation is still warranted.

Because the detection scheme of OCT angiography relies on differences in OCT reflectance or changes in signal phase to highlight blood flow, the images necessarily show movement rather than static features of the retina. Thus, blood flow that is too slow will not be detected above the noise from static tissue, thereby resulting in a loss of visualisation of perfusion in the image. This does not necessarily mean there is a loss of vasculature at these locations; rather blood flow simply could be reduced, there could be no blood flow, or vasculature could be lost. This phenomenon of no visible perfusion is known as the sensitivity limit of OCT angiography and is a function of the time separation between consecutive scans.[36,37] Conversely, flow that is faster than the dynamic range of the decorrelation between

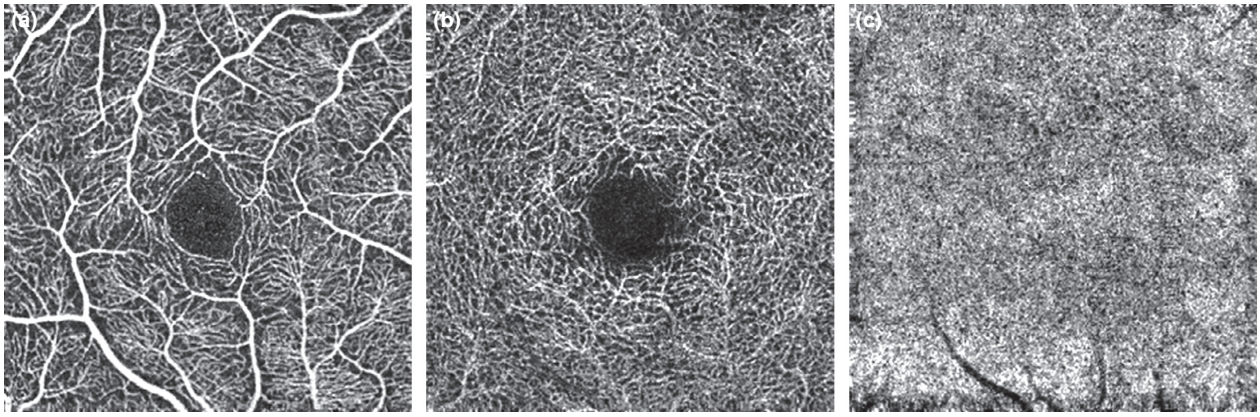

Figure 2. En face OCT angiography scan (nominally 3 × 3 mm using the RTVue-XR Avanti http://www.optovue.com/products/avanti/ and processed with split-spectrum amplitude decorrelation angiography software[34]) of the right eye of a 28 year old normal male demonstrating the visualisation of (a) the superficial retinal plexus, (b) the deep retinal plexus, and (c) the choriocapillaris.[56] Figure courtesy of: Rosen, R.B. (Department of Ophthalmology, New York Eye and Ear Infirmary of Mount Sinai, New York).

adjacent B-scans will saturate the image. Thus, quantification of retinal blood velocity using OCT angiography is difficult. The sensitivity limit of detecting slow flow can be adjusted, with a resulting trade-off in the saturation limit, by utilising variable inter-scan time analysis methodologies such as comparing the reflectance difference between every other scan rather than consecutive scans.[36]

Clinical applications of optical coherence tomography angiography

Despite these caveats, studies using OCT angiography are increasingly being directed at clinical applications. OCT angiography has been used by several investigators to characterise the foveal avascular zone in normal sighted individuals.[39–42] These studies have found that OCT angiography allows for the separation of the superficial vascular plexus and the deep vascular plexus[43,44] and that the foveal avascular zone is larger in the deep plexus than in the superficial plexus.[39] A study by Shahlaee *et al.*[45] found good inter-observer agreement in measuring foveal avascular zone area in the superficial vascular plexus, but more variability in the deep vascular plexus.

Optical coherence tomography angiography is also being applied to cases of disease affecting retinal and choroidal vasculature, such as diabetic retinopathy[46–49]. Several studies have shown foveal avascular zone remodelling and capillary nonperfusion in diabetics even without a clinical diagnosis of diabetic retinopathy.[50–52] For example, the foveal avascular zone was enlarged in diabetic eyes compared to normal,[51–54] with more pronounced differences in the deep vascular plexus than in the superficial vascular plexus.[55] Diabetics displayed a reduced vascular perfusion density and the magnitude of this reduction correlated with increasing severity of diabetic retinopathy.[56]

Microaneurysms show variable visibility on OCT angiography when compared with fluorescein angiography. In some cases, microaneurysms are more clearly visible in OCT angiography than in fluorescein angiography, particularly when they were located in the deep capillary plexus.[47] But in other cases, microaneurysms seen on fluorescein angiography were not visible with OCT angiography.[49] Both of these situations likely result from the detection schemes inherent to OCT angiography; microaneurysms which do not appear on OCT angiography likely are made up of slow blood flows which are below the sensitivity limit for detection. On the other hand, the signal coming from microaneurysms in the deep vascular plexus have been separated from the signal originating from the superficial vascular plexus on OCT angiography. These same microaneurysms on fluorescein angiography may be partially masked by the superficial vascular signal, thereby resulting in their increased visibility on OCT angiography. With these initial results in hand, future studies will almost certainly look at the risk of developing diabetic retinopathy that is associated with early diabetic vascular abnormalities, and the risk of progressing to advanced diabetic retinopathy.

Optical coherence tomography angiography also has been used to examine both non-exudative[36,38,52] and exudative[52,57–64] age related macular degeneration (AMD). Investigators have used OCT angiography to show choroidal neovascularisation (CNV) that penetrates the RPE decreases with anti-vascular endothelial growth factor (anti-VEGF) treatment.[65] Anti-VEGF in these cases leads to a decrease in CNV area and loss of the smaller CNV vessels, yet the central feeder vessels remain present.[66–69] In addition, frequent monitoring of CNV following anti-VEGF treatment using OCT angiography detected the decrease in and subsequent reappearance of CNV at the location of the remaining feeder vessel (*Figure 3*).[70] Conversely, type 1 CNV, which is located beneath and does not penetrate the retinal pigment epithelial (RPE), did not change on OCT angiography following anti-VEGF treatment.[63]

In patients with non-exudative AMD, Palejwala *et al.*[38] detected early CNV on OCT angiography without corresponding dye leakage in fluorescein angiography in two percent of study eyes. Taken together with the results from exudative AMD, these studies suggest that future applications of OCT angiography will include monitoring for the appearance and reappearance of CNV, with the goal of determining the best time interval for delivering more permanent treatments for CNV.[70] Future studies also will certainly look into the risk of progression from non-exudative to exudative AMD and test whether OCT angiography can provide early identification of patients who should be monitored closely to ensure appropriate intervention is given prior to vision loss from exudative AMD.

Optical coherence tomography angiography has also been used to evaluate blood vessel perfusion in numerous retinal and ONH conditions including: subretinal fibrosis,[71] macular telangiectasia,[72–76] idiopathic CNV,[77] punctate inner choroidopathy,[78] polypoidal choroidal vasculopathy,[79] polypoidal choroidal neovascularisation,[79] pachychoroid neovasculopathy,[80] sickle cell maculopathy,[81] retinal vein occlusion,[82–86] retinal artery occlusion,[53,87] acute macular neuroretinopathy and paracentral acute middle maculopathy,[88,89] type 2 retinal arteriovenous malformation,[90] radiation retinopathy,[91] ocular toxoplasmosis,[92] central serous chorioretinopathy,[93–95] choroideremia,[52] birdshot chorioretinopathy (*Figure 4*),[96] hyperoxia,[97] and multiple sclerosis,[98] and glaucoma. In open angle glaucoma, OCT angiography showed reduced vessel flow and density in the optic disk compared to normal, which correlated with glaucoma severity.[99] Similarly, other studies have shown reduced peripapillary capillaries in glaucoma[100] and reduced

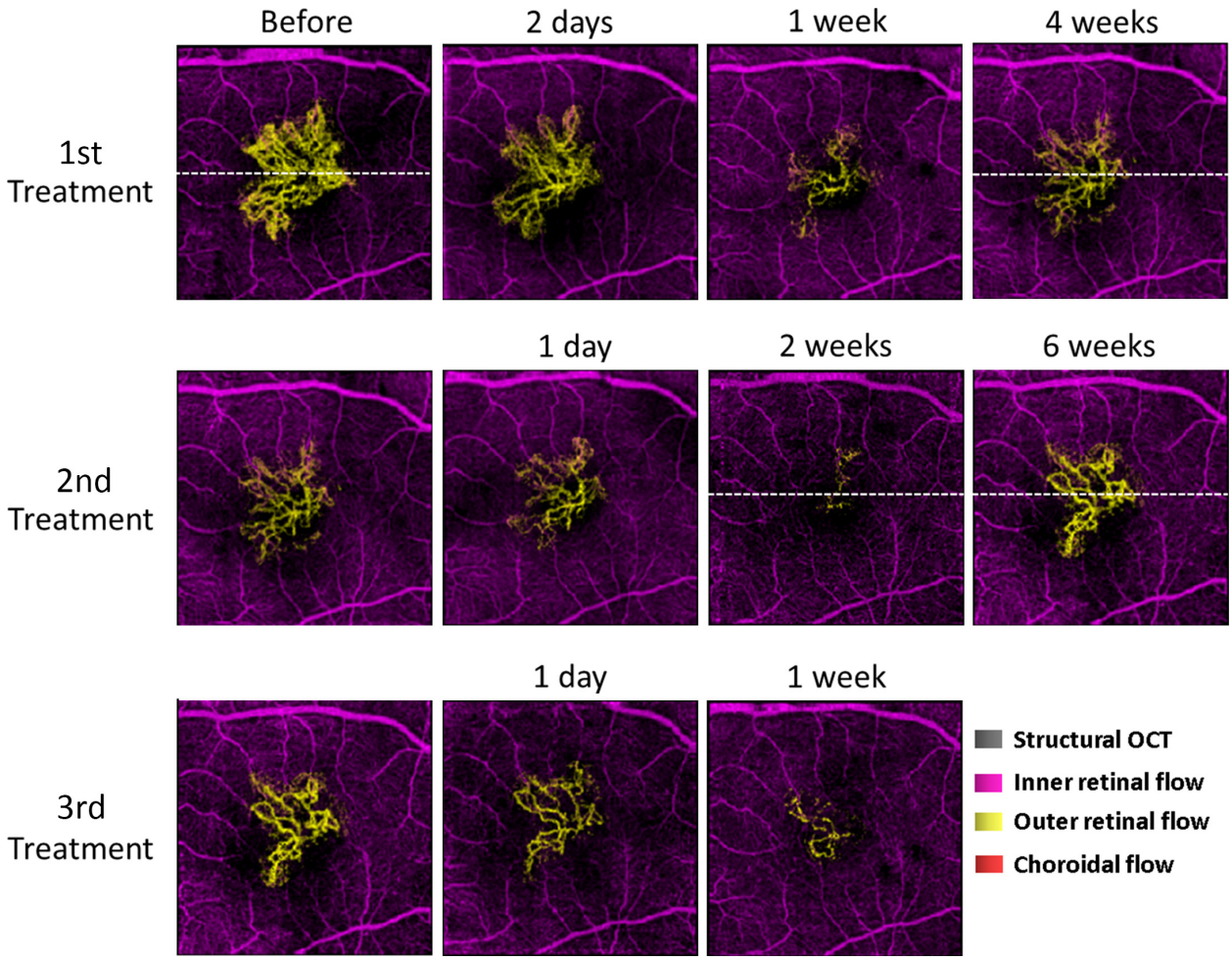

Figure 3. En face OCT angiography scans (nominally 3 × 3 mm OCT scans exported from commercially available RTVue-XR Avanti http://www.optovue.com/products/avanti/ and processed with custom software) from one patient at multiple time points before and following three antiangiogenic treatments of exudative CNV with intravitreal aflibercept injections.[70] In this case, OCT angiography showed the short-term successful response to antiangiogenic treatment and the subsequent reoccurrence of CNV over multiple treatment cycles. The authors suggest that future studies using OCT angiography are needed to determine if OCT angiography can provide a method for individualising the proper antiangiogenic treatment interval such that fluid re-accumulation from CNV does not occur. Figure courtesy of: Huang D, Jia Y, Rispoli M, Tan O, and Lumbroso B. (Casey Eye Institute, Oregon Health and Science University, Portland, Oregon and Centro Oftalmologico Mediterraneo, Rome, Italy). Reprinted from Huang *et al.*[70] with permission from Brucker AJ, editor of RETINA.

perfusion in the optic disk.[101] Beyond a doubt, future studies in this rapidly growing field will utilise OCT angiography to evaluate abnormalities of perfusion in the retinal, choroidal and ONH vascular layers.

Certainly, OCT angiography in its current form does not fully replace fluorescein angiography. Indeed, fluorescein angiography remains superior to OCT angiography for detecting slow blood flow and vessel leakage, due to the sensitivity limit of OCT angiography. However, OCT angiography does have superior capabilities compared to fluorescein angiography in resolving depth features of vascular layers and allowing the direct visualisation of posterior vascular patterns that otherwise may be masked by leakage on fluorescein angiography. Further, the visualisation of vascular perfusion through OCT angiography does not require the application of any external contrast agent. Wide spread clinical utility of OCT angiography will ultimately depend on the availability of OCT imaging systems that include angiography protocols with fast and reliable data interpretations. Some of these algorithms, such as automated detection of CNV,[102] are already under development. It is likely that clinical applications of OCT angiography will only increase as more investigators become familiar with the technique and as image interpretation becomes less arduous and time consuming.

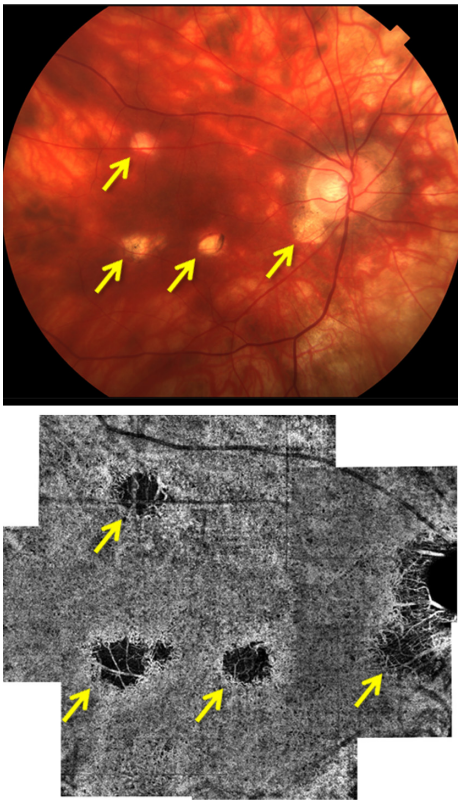

Figure 4. Fundus photography and corresponding OCT angiography (prototype AngioVue OCT angiography software used with the commercially available RTVue-XR Avanti http://www.optovue.com/products/avanti/) montage of the choriocapillaris blood flow in a patient with birdshot chorioretinopathy showing decreased blood flow at the birdshot lesions (arrows). Figure courtesy of: De Carlo TE, Bonini Filho MA, Adhi M and Duker JS (New England Eye Center and Tufts Medical Center, Tufts University, Boston, Massachusetts). Reprinted from De Carlo *et al.*[96] with permission from Brucker AJ, editor of RETINA.

Recently developed spectral domain optical coherence tomography techniques that elucidate previously undetected structure

Despite SD-OCT being a commonly used technique in clinical settings world-wide, investigators are still finding innovative ways to visualise retinal and ONH structures that were previously unmeasurable or undetectable. For example, when first introduced by Spaide *et al.*,[103] enhanced depth imaging OCT (EDI-OCT) was accomplished simply by inverting the SD-OCT image. This allowed enhanced visualisation of the choroid and accurate measurements of choroidal thickness. In this manner, EDI-OCT has been used in recent years to evaluate choroidal health in numerous retinal conditions.[104] SD-OCT has also been used to examine and better quantify ONH structure, and has enabled new assessments of glaucoma detection and risk profiling such as the anterior lamina cribrosa surface depth[105,106] and Bruch's Membrane opening minimum rim width.[107,108] Another example is direction sensitive OCT, which allows direct visualisation of Henle's fibre layer separate from the outer nuclear layer simply by shifting the entry position of the SD-OCT beam laterally away from the centre of the pupil.[109] This technique thereby allows accurate measurement of the outer nuclear layer.

Adaptive optics optical coherence tomography (AO-OCT)

While OCT provides subcellular resolution in the axial direction, its transverse resolution is still limited by the ocular aberrations of the eye. As already described, AO is an optical technique by which the eye's aberrations are corrected and diffraction limited resolution in the transverse direction is obtained. Thus, AO in combination with OCT[17] allows for subcellular resolution in all three spatial directions. Reviews specific to AO-OCT are available.[110,111] Briefly, the AO-OCT technique has allowed for three-dimensional imaging of individual cone photoreceptors (*Figure 5*)[112,113] as well as rod photoreceptors,[113] measurements of individual cone photoreceptor outer segment lengths,[114] visualisation of retinal nerve fibre bundles,[115] images of pores within the lamina cribrosa of the optic nerve,[116,117] and retinal vasculature.[118] Adaptive optics has even been combined with Doppler OCT, resulting in AO-OCT angiography, to allow enhanced vasculature imaging, in particular in the choriocapillaris.[119] Future applications will certainly use AO-OCT to investigate the cellular pathogenesis of retinal disease.

Adaptive optics scanning laser/light ophthalmoscopy (AOSLO)

As mentioned previously, AO has been applied to fundus photography[15] and SLO[16] as well as OCT.[17] To date, AOSLO imaging has enabled the visualisation of more individual retinal cell types than any other retinal imaging modality. As a result, the majority of advanced clinical applications utilising AO have come from AOSLO systems. This review provides a summary of the detection schemes employed for imaging different retinal cell classes and the associated clinical applications that have ensued.

Confocal AOSLO

Adaptive optics scanning laser/light ophthalmoscopy, first described in 2002 by Roorda *et al.*,[16] works by focusing an aberration-corrected spot of light to the retina, and raster scanning that spot quickly over a retinal area. Light reflected (or fluorescently emitted) from the spot is then collected in a point by point fashion over time and

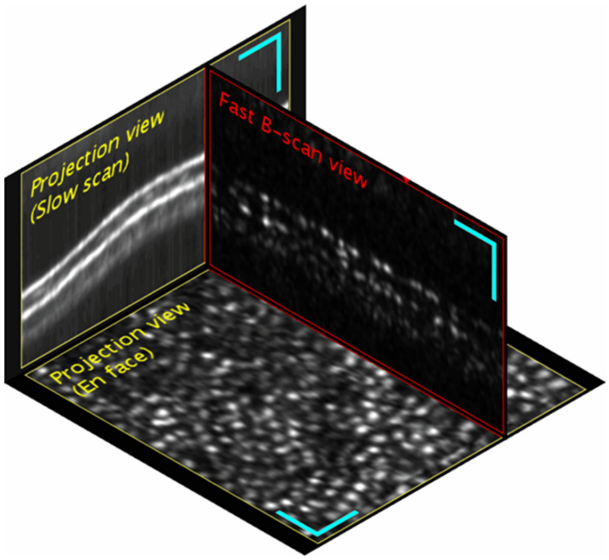

Figure 5. Adaptive optics optical coherence tomography images from a normal control showing the B-scan, en face, and projection views from the volume data set corresponding to the outer retinal layers at 6° superior to the fovea. Individual cone photoreceptors are resolved in three dimensions, allowing measurements of individual cone outer segment lengths in the B-scan image as well as visualisation of the cone mosaic in the en face view. Scale bar 25 μm. Figure courtesy of: Kocaoglu OP, Turner TL, Lui Z and Miller DT (School of Optometry, Indiana University, Bloomington, Indiana).

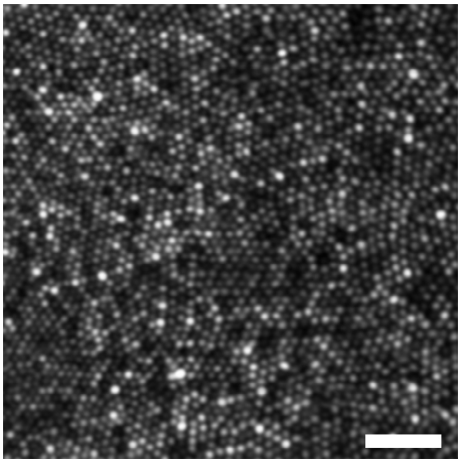

Figure 6. Confocal AOSLO image showing the normal parafoveal cone outer segment mosaic at 0.2 mm temporal retina. Scale bar: 25 μm.

constructed into a spatial image corresponding to the retinal or ONH area illuminated by the scanned light. Coarse optical sectioning is attained by placing a confocal pinhole at a plane optically conjugate with the retina or ONH and in front of a light detection device, for example a photomultiplier tube (PMT). The size of the pinhole, whose purpose is to increase image contrast by rejecting light scattered from areas in front of and behind the plane of focus, dictates the theoretical axial resolution of the AOSLO system as well as the amount of light reaching the detector; diffraction limited systems operating with just over one Airy disk sized pinholes attain axial resolutions of approximately 50 μm.[120] Clinical applications utilising this combination of confocal optical sectioning, AO, and SLO technologies were immediately recognised. In the first paper introducing this technology, Roorda *et al.*[16] reported visualisation of the nerve fibre layer, retinal blood flow, and the cone photoreceptor mosaic.

Since this ground-breaking work by Roorda *et al.*,[16] confocal reflectance AOSLO imaging has been applied to basic and clinical ophthalmic research for visualisation of numerous features in both normal and diseased retina and ONH. For example, the waveguided reflectance signal emanating from the cone photoreceptor outer segments (*Figure 6*) has proven to be one of the more salient and quantifiable features of confocal AOSLO (and AO flood-illumination) imaging, as is evident by the high number of publications dedicated to characterising this signal in various stages of retinal health and disease. Recent studies have shown the topography of the normal cone mosaic[121,122] and repeatability in cone density measurements made from these AOSLO images.[123] Characterisation of the cone outer segment mosaic has been performed in numerous diseases including (but nowhere near limited to): AMD,[124–133] glaucoma,[134] diabetic retinopathy,[135,136] retinitis pigmentosa,[137–143] Stargardt's,[144,145] choroideremia,[146,147] achromatopsia,[148–150] macular telangiectasia,[151–154] and central serous chorioretinopathy.[155] Of interest from this group of literature as a whole, is the observation that the cone outer segment mosaic exhibits different characteristics in a disease dependent manner; for example, the parafoveal cone outer segments are present in choroideremia with generally the proper density, however their reflectance is overall dimmer and of poorer quality than the normal cone mosaic.[147] In contrast, parafoveal cone spacing in Stargardt's is increased (resulting in decreased cone density),[144] while in achromatopsia the cone outer segments are dim or not visible (either because they are not present or not properly waveguiding).[148] The ability to characterise how and why the waveguided cone outer segment signal changes in different disease conditions may lead to a better understanding of the underlying mechanisms causing retinal disease.

Rod outer segment mosaic imaging has proven more difficult than cone imaging, in part because rod size is very close to the diffraction limit of the dilated pupil (rods are approximately 2–3 μm in diameter in comparison to cones which range from 2–3 μm at the fovea to 8 μm or larger in the periphery[156]) and the waveguided signal emanating

from the rods is more broadly tuned. It took almost a decade to optimise AO systems such that the normal rod outer segment mosaic could be visualised.[157–162] With this capability now in hand (*Figure 7*), researchers are again applying this relatively recent technological advance to study rod involvement in retinal disease at the cellular level.[145,163–165]

Another cell layer absolutely critical for maintaining retinal health is the retinal pigment epithelium (RPE). The RPE is a monolayer of cells that sits directly posterior to the photoreceptor outer segments. It serves as the blood retinal barrier in the eye, participates in the visual cycle to regenerate 11-cis retinal following photo-isomerization, and provides metabolic support to the photoreceptors.[166] Confocal reflectance AOSLO imaging has enabled visualisation of the RPE cells but only in cases of retinal disease where signal from the photoreceptors is no longer present.[167,168] Visualisation of the normal RPE in confocal AOSLO has remained elusive because the cone and rod photoreceptor signal overwhelms any confocal reflectance signal originating from the RPE and the axial resolution of AOSLO precludes optical sectioning of these adjacent cell layers. Other AOSLO detection schemes such as autofluorescence[169] and dark-field[170] (described below) have proven more robust for non-invasive observation of the normal and diseased RPE.

Adaptive optics scanning laser/light ophthalmoscopy imaging systems acquire individual frames anywhere from approximately 15 frames per second to hundreds of frames per second thereby allowing real-time movies of the retina to be recorded. Blood flow through the retinal vessels becomes immediately noticeable in AOSLO movies,[16] especially once the frames are co-registered and stabilised to compensate for any fixational eye motion.[171] Indeed, AOSLO imaging allows for the observation of retinal vasculature and blood flow through even the finest retinal capillaries without adding invasive contrast agents, such as fluorescein.[172–175] Like OCT angiography, further contrast of retinal vessels can be obtained by analysing residual differences between consecutive frames in the AOSLO stabilised movie, and attributing these differences to blood flow through the retinal vessels. The result is a motion contrast image, or perfusion map just like OCT angiography, which highlights areas in the retina where blood flow is observed.[174,176] In this manner, AOSLO imaging has also been used to study the normal and diseased retinal vasculature and the avascular zone surrounding the anatomical fovea.[177–184] In comparison with OCT angiography, AOSLO vascular perfusion maps consist of a combination of the superficial and deep vascular plexus and have not allowed visualisation of choroidal blood flow unless retinal window defects are present.

Finally, the nerve fibre layer[185–189] and the lamina cribrosa of the optic nerve[190–192] have been examined by confocal reflectance AOSLO imaging. The nerve fibre layer consists of bundles of ganglion cell axons which originate from the ganglion cell body and traverse the anterior side of the retina, where they exit the eye through the optic nerve. The lamina cribrosa is a porous structure in the optic nerve that the nerve fibres and retinal vasculature pass through (*Figure 8*). Both of these retinal features are affected in glaucoma; Akagi *et al.*[191] found that the size of the laminar pores were increased in 20 glaucoma eyes compared to normal, and numerous AO studies have shown nerve fibre layer loss in glaucoma patients.[186–189] Future clinical applications of AOSLO imaging technology will certainly include the study of these structures in larger numbers of at risk patients and in treated cases of glaucomatous eyes.

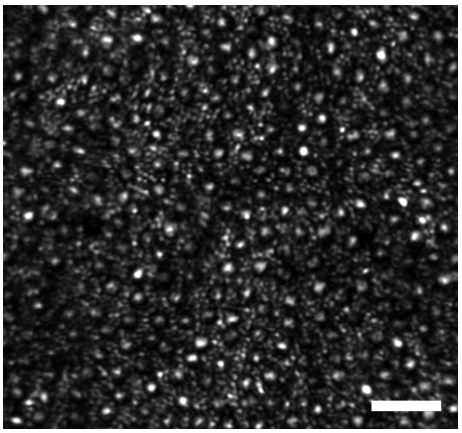

Figure 7. Confocal AOSLO image showing the normal cone and rod outer segment mosaic at 10° temporal to fixation. Scale bar: 25 μm. Figure courtesy of: Scoles D and Dubra A. (Department of Biomedical Engineering, University of Rochester, Rochester, New York and Department of Ophthalmology, Medical College of Wisconsin, Milwaukee, Wisconsin).

Fluorescence AOSLO

The clinical utility of confocal AOSLO was expanded with the incorporation of fluorescence imaging techniques to AOSLO imaging systems.[193] In this detection scheme, the retina is illuminated using a short wavelength light source (typically anywhere from 488 to 568 nm) to excite intrinsic or inserted fluorophores, and chromatic filters are placed in the detection arm of the system such that the point detectors collect light emitted at wavelengths longer than the excitation wavelength. Fluorescence imaging is limited by the availability of fluorophores within the retina. AOSLO in combination with fluorescein angiography has shown the finest retinal capillaries in both normal and diseased retina along with abnormal vascular changes

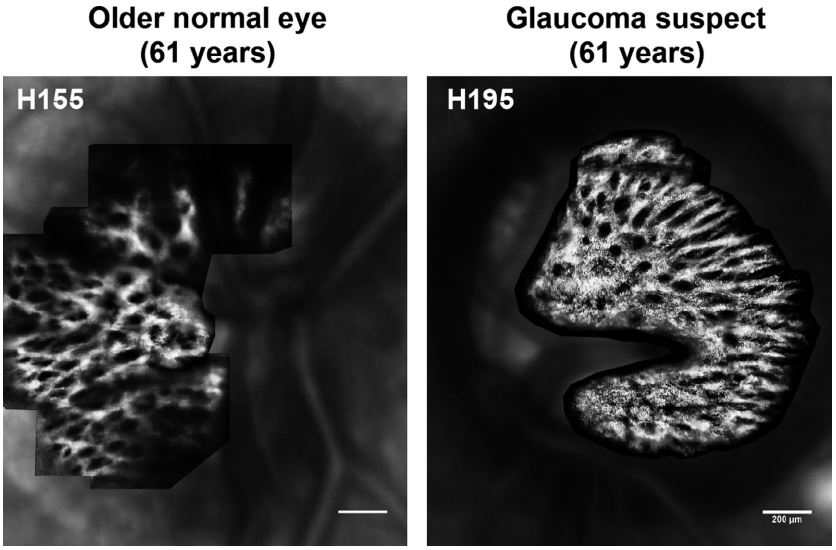

Figure 8. Confocal AOSLO images of the lamina cribrosa in a normal subject and a glaucoma suspect patient overlaid on a non-AO SLO image of the nerve. Scale bars: 200 µm. Figure courtesy of: Bhakta AS, Marrelli DJ, and Porter J (College of Optometry, University of Houston, Houston, Texas).

such as microaneurysms in diabetes and hypertension (*Figure 9*).[194–198]

Adaptive optics scanning laser/light ophthalmoscopy autofluorescence imaging has taken advantage of the intrinsic fluorescence of lipofuscin granules within the RPE cells.[199] The spatial arrangement of lipofuscin located in the RPE cell cytoplasm but not the cell nucleus provides contrast in the autofluorescence image. Autofluorescence imaging, when combined with the high transverse resolution afforded by AOSLO imaging, allows visualisation of the RPE mosaic in both normal and diseased retina (*Figure 10*).[169,170,200–202] In addition, autofluorescence AOSLO imaging has enhanced our understanding of retinal phototoxicity,[203–205] the result of which has established new American National Standards Institute (ANSI) guidelines for the Safe Use of Lasers in ocular exposures.[206]

Non-confocal AOSLO

For more than a decade AOSLO was used only in confocal detection mode, thereby excluding multiply scattered and defocused light from reaching the detectors. This changed in 2012 when Chui *et al.*[207] used an offset pinhole (a pinhole translated from the confocal location to block the

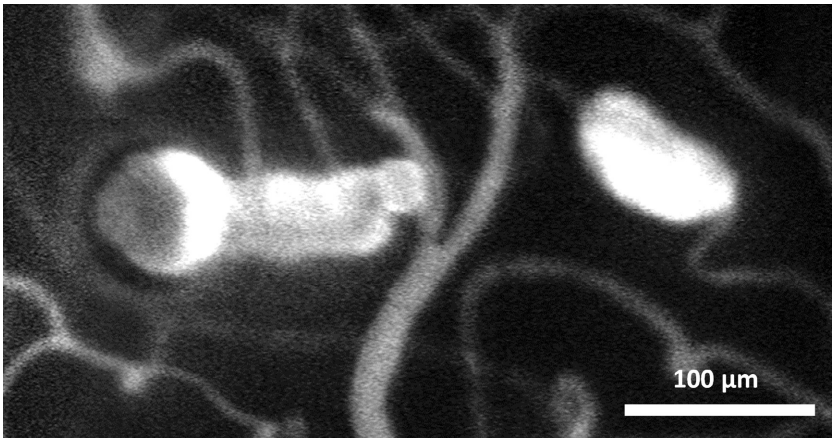

Figure 9. Fluorescein pooling and blood flow pattern of two microaneurysms located at 2° temporal to the fovea in a 47 year old male with hypertensive retinopathy. Figure courtesy of: Chui TY and Rosen RB (Department of Ophthalmology, New York Eye and Ear Infirmary of Mount Sinai, New York). Reprinted from Chui *et al.*[196] with permission from the Optical Society of America.

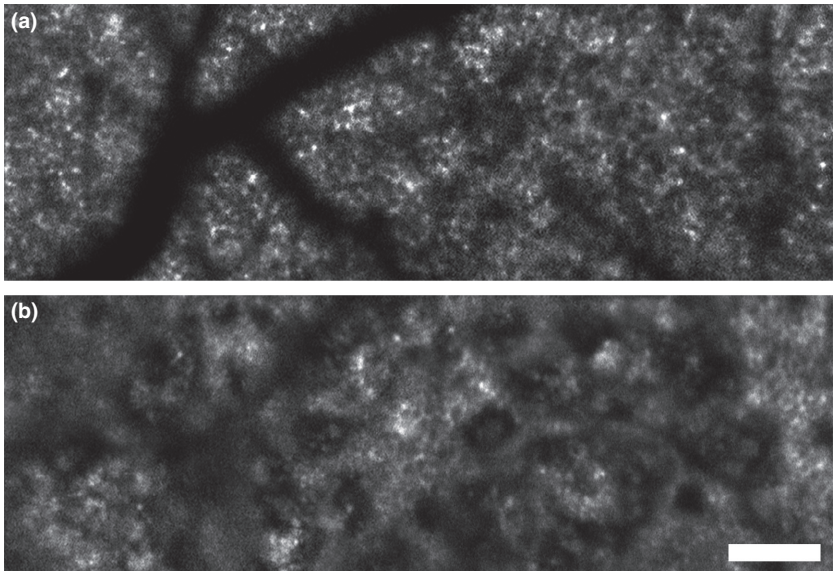

Figure 10. Autofluorescence AOSLO images depicting the lipofuscin within the RPE cell mosaic in a 41 year old normal subject (a) and a patient with cuticular drusen (b) located 1.5 mm temporal to fixation. Scale bar: 100 μm. Figure courtesy of: Rossi EA, Song H, Yang Q, Granger C, Latchney LR, Williams DR and Chung MM (Center for Visual Science, University of Rochester, Rochester, New York).

confocal signal and instead collect multiply scattered light) to increase the visibility of retinal vasculature.[208] The resulting images acquired under offset pinhole conditions led to the incorporation of other non-confocal microscopy detection schemes with AOSLO imaging technology. In two high impact studies,[170,209] Scoles *et al.* described two different non-confocal detection techniques, each of which represent a major advance for non-invasive cellular imaging in the retina. In the first, Scoles *et al.*[170] blocked the confocal reflectance signal, and instead collected the light passing through an annulus surrounding the confocal signal. Termed 'dark-field,' the resulting images elucidated the RPE cells, by optically blocking the waveguided signal from the overlaying photoreceptors (*Figure 11*). This technique has the major advantage of allowing visualisation of the RPE cells under near infrared (IR) illumination conditions, which is both safer and more pleasant for patient viewing than the autofluorescence illumination techniques that typically require illumination in the middle wavelength portion of the visible spectrum where the safety limits are more restrictive and the eye is most sensitive. However, dark-field AOSLO imaging cannot fully replace autofluorescence imaging for investigating RPE health, as the signal arising from visible autofluorescence is caused by the presence of lipofuscin, whose quantity is known to change in retinal disease.[210]

The second non-confocal detection technique described by Scoles *et al.*[209] arises from split detection microscopy. In this detection scheme, the confocal signal is blocked (or separated by a mask) from the multiply scattered non-confocal

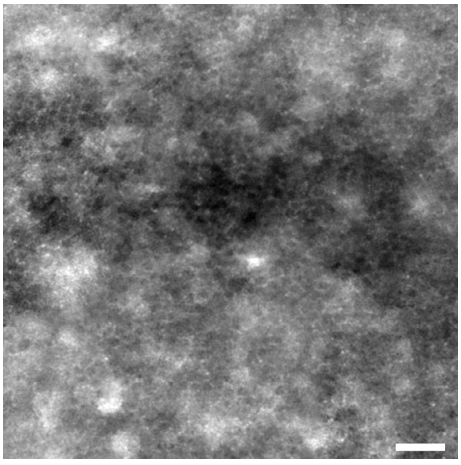

Figure 11. Dark-field AOSLO image showing the normal RPE cell mosaic at the fovea. Scale bar: 50 μm. Figure courtesy of: Cooper RF and Dubra A (Department of Biomedical Engineering, Marquette University, Milwaukee, Wisconsin and Department of Ophthalmology, Medical College of Wisconsin, Milwaukee, Wisconsin).

signal, just as in the dark-field detection scheme. The non-confocal annular signal is then divided (split) into two semi-annular signals, each of which is collected by a separate detector. The algorithm for the split detection image is then simply the difference of the two semi-annular signals divided by the sum. By using this technique, Scoles *et al.*[209] successfully imaged the cone photoreceptor inner segments in both normal sighted controls (*Figure 12*) and in patients with achromatopsia. These images demonstrated that the

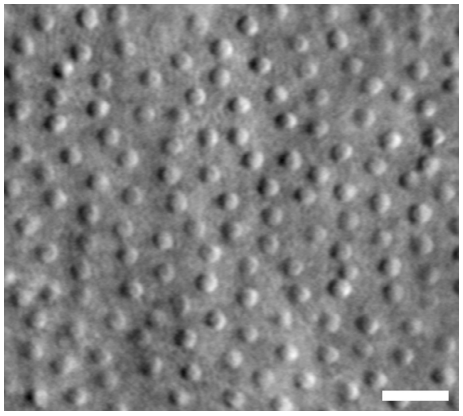

Figure 12. Split detection AOSLO image showing the normal cone inner segment mosaic at 20° temporal to fixation. Scale bar: 25 μm. Figure courtesy of: Scoles D and Dubra A (Department of Biomedical Engineering, University of Rochester, Rochester, New York and Department of Ophthalmology, Medical College of Wisconsin, Milwaukee, Wisconsin).

split detection technique is a method that can provide contrast between cells that are otherwise transparent in confocal AOSLO imaging. In addition, this paper shows that loss of visible, waveguiding cone outer segments does not necessarily mean loss of the cone cell body; in the patients with achromatopsia cone inner segments remained present in retina locations corresponding to loss of outer segment reflectance. Another beautiful feature of the split detection imaging technique is that by incorporating three point detectors into the AOSLO system, investigators are able to collect confocal, dark-field, and split detection images simultaneously, which therefore allows investigators to compare photoreceptor inner segments, photoreceptor outer segments, and RPE cells at the same spatial location.

Split detection AOSLO imaging has also been applied for high resolution observation of retinal vasculature.[211] The increased contrast afforded by split detection allows superior observation of retinal vessel walls, endothelial cells, pericytes, and blood flow. Motion contrast image processing as described above with confocal imaging enhances the visualisation of retinal perfusion under split detection schemes as well.

Longitudinal cellular imaging as an assessment of disease progression and treatment efficacy

Naturally following the ability to observe individual retinal cells noninvasively, comes the desire to follow the health of individual cells over an extended period of time. Prior to AO imaging, the only way to assess retinal disease at an individual cellular level was through cross-sectional studies using histological preparations. Histology presents numerous problems including inter-subject variability, lack of patient samples, in particular samples from young individuals with early stage disease, and changes induced by fixation and dissection techniques, just to name a few. *In vivo* AO imaging circumvents the problems encountered in histological preparations; investigators can use AO techniques to return to the same retinal location at multiple time points and thereby follow the health of individual cells even over years. Longitudinal imaging with AO has been demonstrated in the normal and diseased retina to track the photoreceptors,[212] RPE cells,[169] and retinal vasculature.[179] Future studies almost certainly will use this technology to assess disease progression at the cellular level by tracking the survival and loss of individual cells over time (*Figure 13*).

The capability of imaging the same retinal location with cellular resolution at multiple time points, gives

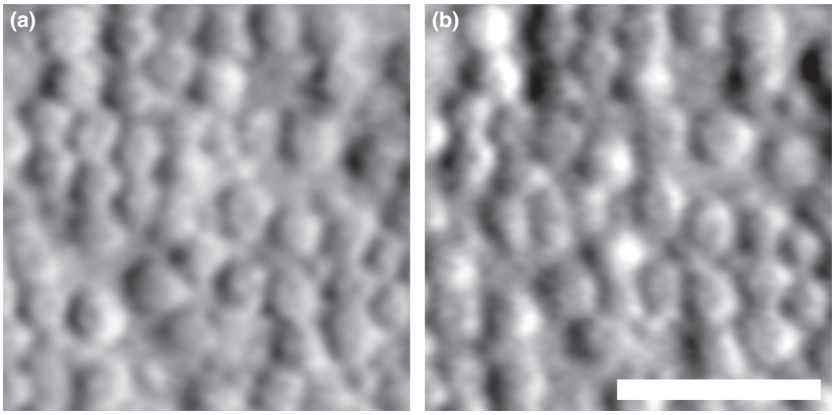

Figure 13. Split detection AOSLO image showing the foveal cone inner segment mosaic in a patient with achromatopsia at the baseline visit (a) and 1 year later (b), illustrating the capability of longitudinal imaging at the cellular level. In this case, the same cone inner segments are visible at the same retinal location, showing stability of the cone mosaic for this patient over 1 year. Scale bar: 25 μm. Figure courtesy of: Langlo CS, Dubra A, and Carroll J (Department of Ophthalmology, Medical College of Wisconsin, Milwaukee, Wisconsin).

investigators the unique opportunity to assess how a cell, or group of cells, respond to disease intervention. Despite this enticing possibility, to my knowledge there has only been one peer-reviewed publication to date using AOSLO imaging to assess photoreceptor health in response to an experimental treatment. In this study, Talcott *et al.*,[212] measured cone density in three eyes treated by a ciliary neuro-trophic factor (CNTF) implant compared with sham-treated control eyes and normal sighted control eyes. They found that cone density in the sham-treated eye decreased significantly faster over 24 months as compared to the CNTF treated eye. These results suggest that cellular imaging can be a highly sensitive way to measure both disease progression as well as treatment efficacy. Despite the CNTF implant treated eyes maintaining higher cone densities than the sham-treated eyes, the unmasked results of a larger Phase 2 CNTF study showed the CNTF implant had no therapeutic benefit as determined by the primary outcome measures of visual acuity and visual field sensitivity.[213] Taken together, these results hint that AOSLO imaging of cone structure may show treatment efficacy on a shorter time scale than measures of visual acuity and visual field sensitivity, or alternatively, that slowing the decrease of visible cones in AOSLO images may not lead to a functional benefit for patients.

Either way, the results from Talcott *et al.*[212] certainly will encourage more studies to test cellular imaging as an outcome measure for experimental treatments of retinal disease. For one thing, the capability to assess treatment efficacy on a faster time scale than is currently available would enhance treatment development by reducing the cost and time required to run clinical (and preclinical) trials. Further, while the general rule of thumb stipulates that clinical trials require a functional measure of vision as the primary outcome variable, exceptions can be made for structural outcomes that are shown to correlate with functional results. One example is the size of geographic atrophy in age-related macular degeneration, as an increase in geographic atrophy is known to cause loss of the photoreceptors and therefore cause a decrease in visual function.[214] More studies are needed to correlate imaging data showing longitudinal cell survival and loss with remaining visual function. Despite the lack of this data to date, current understanding of the visual system would dictate that preserving retinal structure at the cellular level, such as was observed in the AO CNTF study, remains a positive outcome.

Functional assessment of the retina using AOSLO and OCT imaging techniques

The same AO ophthalmoscopy techniques that enable high-resolution retinal imaging also have been used for presenting an aberration corrected visual stimulus to the retina to test subjective visual function, such as color appearance[215] and visual acuity,[216] in comparison with retinal structure. Investigators have also developed techniques to allow microperimetry through the AO system. One benefit of AOSLO microperimetry is that investigators can conduct functional assessments of the visual system while also simultaneously imaging the retina and therefore can determine exactly where on the retina a stimulus falls. In this manner, investigators have used AO microperimetry techniques to test the light sensitivity of individual and small groups of cones as well as the function of local retinal lesions.[168,217–219] Of importance, Wang *et al.*[168] have shown in patients with macular telangiectasia that locations within AO confocal images that do not show the cone mosaic and do not show reflections on OCT corresponding to photoreceptor layers, can still retain cone function measured through psychophysical responses to visible stimuli. This finding has challenged the idea that photoreceptor structure must be visible in confocal AOSLO images for the retinal location to retain function.

While a gold standard for assessing the preservation of individual photoreceptor function can be provided using cell-by-cell microperimetry, testing vision one cell at a time is not practical, in particular for studies which aim to assess either a high number of cells or a high number of patients. Instead, an appealing alternative is to use retinal imaging techniques to assess individual cellular function without requiring a subjective response from study participants. To do this, investigators must first identify functional imaging biomarkers and then validate that these biomarkers correlate to physiological function.

Early work on this endeavour has been started using both OCT and AO imaging techniques to identify visual stimulus induced responses in both photoreceptors and blood flow. Indeed, initial results in frog,[220] rabbit,[221] and rat[222] retina showed intrinsic optical changes in near-infrared backscattering on OCT following the onset of a visible light stimulus. Srinivasan *et al.*[223] pioneered a functional OCT study in humans noninvasively and demonstrated a stimulus induced change in OCT backscattering occurred in retinal layers corresponding to the inner segment/outer segment (IS/OS) junction and the rod outer segment tips.

With the encouraging results from OCT showing reflectance changes co-localised with the photoreceptor layers, investigators have begun using the same general methods to investigate stimulus evoked intrinsic optical signals in single cells through en face AO imaging. Several studies have now shown that the signal arising from the cone outer segment reflectance changes following a visible stimulus.[224–226] Despite these observations, the cause of the reflectance changes remains unclear. One model predicts

for long coherence length imaging sources that the stimulus evoked signal is caused by a change in interference between the IS/OS junction and the cone outer segment tips that arises because of a change in the optical path length between the two layers.[227] More work is needed however to understand the source of these signals, particularly in conditions when the interference model is an incomplete solution such as when the imaging source has a short coherence length relative to the length of the outer segment.[226]

Finally, visual stimuli have been shown to cause changes in blood velocity and blood flow using both AOSLO[228] and OCT angiography[229] techniques. Much more work is needed before investigators identify and understand all the mechanisms involved with stimulus evoked optical responses in the retina. However, the fact remains that the same AO and OCT techniques used to image the photoreceptors and vascular networks non-invasively have the potential to probe retinal function on a cellular scale, objectively.

Summary

Without doubt, the retinal imaging technologies described in this review have enhanced our clinical understanding of the normal and diseased visual system. And while our field's cellular imaging achievements to date are impressive, it is also likely they represent only first steps towards developments to come in basic vision research and ophthalmic medicine. Future studies will certainly continue to utilise OCT and AO capabilities to explore disease pathogenesis and assess disease progression. In addition, researchers are increasingly likely to utilise these imaging techniques for assessing treatment efficacy with high sensitivity, especially as more gene, cell, and small molecule experimental therapies enter into clinical trials. Eventually, these same imaging tools may provide objective criteria to identify groups of patients most likely to benefit from a given treatment and be used to aid in the selection of patients that should enroll in clinical trials testing experimental interventions. For example, gene therapy is most likely to benefit patients whose retinal structure remains intact. Split detection AOSLO imaging may therefore be helpful by identifying which patients have remaining cone cell bodies present and where treatments should be directed in the retina to target these cells.

Finally, while we have come a long way in observing individual cells in the human retina, it is important to remember that the majority of retinal cells (ganglion cells, amacrine cells, horizontal cells, müller cells, and biopolar cells) currently remain undetectable. Certainly investigators will continue to develop innovative imaging methodologies aimed at producing the contrast necessary to visualise these transparent cells noninvasively in humans.

In conclusion, it is fair to say that like the fundus photo and fluorescein angiogram, OCT and AO ophthalmoscopy are here to stay.

Acknowledgements

This manuscript was supported by NIH U01EY025477, NIH U01EY025864, the Foundation Fighting Blindness, Research to Prevent Blindness, the F. M. Kirby Foundation, and the Paul and Evanina Mackall Foundation Trust. The content is solely the responsibility of the author and does not necessarily represent the official views of the National Institutes of Health.

Disclosure

JIWM holds US Patent 8226236 on material related to this review.

References

1. Jackman W & Webster J. Photographing the retina of the living human eye. *Photogr News* 1886; 23: 340–341.
2. Marmor MF & Ravin JG. Fluorescein angiography: insight and serendipity a half century ago. *Arch Ophthalmol* 2011; 129: 943–948.
3. Novotny HR & Alvis DL. A method of photographing fluorescence in circulating blood in the human retina. *Circulation* 1961; 24: 82–86.
4. Fercher AF, Mengedoht K & Werner W. Eye-length measurement by interferometry with partially coherent light. *Opt Lett* 1988; 13: 186–188.
5. Hitzenberger CK. Optical measurement of the axial eye length by laser Doppler interferometry. *Invest Ophthalmol Vis Sci* 1991; 32: 616–624.
6. Huang D, Swanson EA, Lin CP *et al.* Optical coherence tomography. *Science* 1991; 254: 1178–1181.
7. Fercher AF, Drexler W, Hitzenberger CK & Lasser T. Optical coherence tomography – principles and applications. *Rep Prog Phys* 2003; 66: 239–303.
8. Fercher AF, Hitzenberger CK, Kamp G & El-Zaiat SY. Measurement of intraocular distances by backscattering spectral interferometry. *Opt Commun* 1995; 117: 43–48.
9. Wojtkowski M, Leitgeb R, Kowalczyk A, Bajraszewski T & Fercher AF. In vivo human retinal imaging by Fourier domain optical coherence tomography. *J Biomed Opt* 2002; 7: 457–463.
10. Nassif N, Cense B, Park BH *et al.* In vivo human retinal imaging by ultrahigh-speed spectral domain optical coherence tomography. *Opt Lett* 2004; 29: 480–482.
11. Wojtkowski M, Srinivasan V, Ko T *et al.* Ultrahigh-resolution, high-speed, Fourier domain optical coherence tomography and methods for dispersion compensation. *Opt Express* 2004; 12: 2404–2422.

12. Leitgeb R, Hitzenberger C & Fercher A. Performance of Fourier domain vs. time domain optical coherence tomography. *Opt Express* 2003; 11: 889–894.
13. Choma M, Sarunic M, Yang C & Izatt J. Sensitivity advantage of swept source and Fourier domain optical coherence tomography. *Opt Express* 2003; 11: 2183–2189.
14. Yun S, Tearney G, de Boer J, Iftimia N & Bouma B. High-speed optical frequency-domain imaging. *Opt Express* 2003; 11: 2953–2963.
15. Liang J, Williams DR & Miller DT. Supernormal vision and high-resolution retinal imaging through adaptive optics. *J Opt Soc Am A* 1997; 14: 2884–2892.
16. Roorda A, Romero-Borja F, Donnelly WJ III *et al.* Adaptive optics scanning laser ophthalmoscopy. *Opt Express* 2002; 10: 405–412.
17. Hermann B, Fernandez EJ, Unterhuber A *et al.* Adaptive-optics ultrahigh-resolution optical coherence tomography. *Opt Lett* 2004; 29: 2142–2144.
18. Ferrara D, Waheed NK & Duker JS. Investigating the choriocapillaris and choroidal vasculature with new optical coherence tomography technologies. *Prog Retin Eye Res* 2015; http://www.sciencedirect.com/science/article/pii/S1350946215000828 [Available online 23 Oct 2015].
19. Mahmud MS, Cadotte DW, Vuong B *et al.* Review of speckle and phase variance optical coherence tomography to visualize microvascular networks. *J Biomed Opt* 2013; 18: 50901.
20. van Velthoven ME, Faber DJ, Verbraak FD, van Leeuwen TG & de Smet MD. Recent developments in optical coherence tomography for imaging the retina. *Prog Retin Eye Res* 2007; 26: 57–77.
21. Williams DR. Imaging single cells in the living retina. *Vision Res* 2011; 51: 1379–1396.
22. Roorda A. Applications of adaptive optics scanning laser ophthalmoscopy. *Optom Vis Sci* 2010; 87: 260–268.
23. Roorda A. Adaptive optics for studying visual function: a comprehensive review. *J Vis* 2011; 11: 1–21.
24. Godara P, Dubis AM, Roorda A, Duncan JL & Carroll J. Adaptive optics retinal imaging: emerging clinical applications. *Optom Vis Sci* 2010; 87: 930–941.
25. Roorda A & Duncan JL. Adaptive optics ophthalmoscopy. *Annu Rev Vis Sci* 2015; 1: 19–50.
26. Leitgeb R, Schmetterer L, Drexler W *et al.* Real-time assessment of retinal blood flow with ultrafast acquisition by color Doppler Fourier domain optical coherence tomography. *Opt Express* 2003; 11: 3116–3121.
27. Yazdanfar S, Rollins AM & Izatt JA. In vivo imaging of human retinal flow dynamics by color Doppler optical coherence tomography. *Arch Ophthalmol* 2003; 121: 235–239.
28. White B, Pierce M, Nassif N *et al.* In vivo dynamic human retinal blood flow imaging using ultra-high-speed spectral domain optical coherence tomography. *Opt Express* 2003; 11: 3490–3497.
29. Makita S, Jaillon F, Yamanari M, Miura M & Yasuno Y. Comprehensive in vivo micro-vascular imaging of the human eye by dual-beam-scan Doppler optical coherence angiography. *Opt Express* 2011; 19: 1271–1283.
30. Zotter S, Pircher M, Torzicky T *et al.* Visualization of microvasculature by dual-beam phase-resolved Doppler optical coherence tomography. *Opt Express* 2011; 19: 1217–1227.
31. Kim DY, Fingler J, Werner JS *et al.* In vivo volumetric imaging of human retinal circulation with phase-variance optical coherence tomography. *Biomed Opt Express* 2011; 2: 1504–1513.
32. Kim DY, Fingler J, Zawadzki RJ *et al.* Optical imaging of the chorioretinal vasculature in the living human eye. *Proc Natl Acad Sci U S A* 2013; 110: 14354–14359.
33. Schwartz DM, Fingler J, Kim DY *et al.* Phase-variance optical coherence tomography: a technique for noninvasive angiography. *Ophthalmology* 2014; 121: 180–187.
34. Jia Y, Tan O, Tokayer J *et al.* Split-spectrum amplitude-decorrelation angiography with optical coherence tomography. *Opt Express* 2012; 20: 4710–4725.
35. Spaide RF. Volume-rendered angiographic and structural optical coherence tomography. *Retina* 2015; 35: 2181–2187.
36. Choi W, Moult EM, Waheed NK *et al.* Ultrahigh-speed, swept-source optical coherence tomography angiography in nonexudative age-related macular degeneration with geographic atrophy. *Ophthalmology* 2015; 122(12): 2532–44.
37. Spaide RF, Fujimoto JG & Waheed NK. Image artifacts in optical coherence tomography angiography. *Retina* 2015; 35: 2163–2180.
38. Palejwala NV, Jia Y, Gao SS *et al.* Detection of nonexudative choroidal neovascularization in age-related macular degeneration with optical coherence tomography angiography. *Retina* 2015; 35: 2204–2211.
39. Samara WA, Say EA, Khoo CT *et al.* Correlation of foveal avascular zone size with foveal morphology in normal eyes using optical coherence tomography angiography. *Retina* 2015; 35: 2188–2195.
40. Carpineto P, Mastropasqua R, Marchini G *et al.* Reproducibility and repeatability of foveal avascular zone measurements in healthy subjects by optical coherence tomography angiography. *Br J Ophthalmol* 2015; http://www.ncbi.nlm.nih.gov/pubmed/?term=Carpineto+P%2C+Mastropasqua+R%2C+Marchini+G+et+al.+Reproducibility+and+repeatability+of+foveal+avascular+zone. [Available online 16 Sep 2015]
41. Matsunaga D, Yi J, Puliafito CA & Kashani AH. OCT angiography in healthy human subjects. *Ophthalmic Surg Lasers Imaging Retina* 2014; 45: 510–515.
42. Spaide RF, Klancnik JM Jr & Cooney MJ. Retinal vascular layers imaged by fluorescein angiography and optical coherence tomography angiography. *JAMA Ophthalmol* 2015; 133: 45–50.

43. Savastano MC, Lumbroso B & Rispoli M. In vivo characterization of retinal vascularization morphology using optical coherence tomography angiography. *Retina* 2015; 35: 2196–2203.
44. Bonnin S, Mane V, Couturier A *et al.* New insight into the macular deep vascular plexus imaged by optical coherence tomography angiography. *Retina* 2015; 35: 2347–2352.
45. Shahlaee A, Pefkianaki M, Hsu J & Ho AC. Measurement of foveal avascular zone dimensions and its reliability in healthy eyes using optical coherence tomography angiography. *Am J Ophthalmol* 2016; 161: 50–55.
46. Couturier A, Mane V, Bonnin S *et al.* Capillary plexus anomalies in diabetic retinopathy on optical coherence tomography angiography. *Retina* 2015; 35: 2384–2391.
47. Ishibazawa A, Nagaoka T, Takahashi A *et al.* Optical coherence tomography angiography in diabetic retinopathy: a prospective pilot study. *Am J Ophthalmol* 2015; 160: 35–44 e1.
48. Matsunaga DR, Yi JJ, De Koo LO *et al.* Optical coherence tomography angiography of diabetic retinopathy in human subjects. *Ophthalmic Surg Lasers Imaging Retina* 2015; 46: 796–805.
49. Hwang TS, Jia Y, Gao SS *et al.* Optical coherence tomography angiography features of diabetic retinopathy. *Retina* 2015; 35: 2371–2376.
50. de Carlo TE, Chin AT, Bonini Filho MA *et al.* Detection of microvascular changes in eyes of patients with diabetes but not clinical diabetic retinopathy using optical coherence tomography angiography. *Retina* 2015; 35: 2364–2370.
51. Di G, Weihong Y, Xiao Z *et al.* A morphological study of the foveal avascular zone in patients with diabetes mellitus using optical coherence tomography angiography. *Graefe's Arch Clin Exp Ophthalmol* 2015; [Epub ahead of print].
52. Jia Y, Bailey ST, Hwang TS *et al.* Quantitative optical coherence tomography angiography of vascular abnormalities in the living human eye. *Proc Natl Acad Sci U S A* 2015; 112: E2395–E2402.
53. Bonini Filho MA, Adhi M, de Carlo TE *et al.* Optical coherence tomography angiography in retinal artery occlusion. *Retina* 2015; 35: 2339–2346.
54. Takase N, Nozaki M, Kato A *et al.* Enlargement of foveal avascular zone in diabetic eyes evaluated by en face optical coherence tomography angiography. *Retina* 2015; 35: 2377–2383.
55. Freiberg FJ, Pfau M, Wons J *et al.* Optical coherence tomography angiography of the foveal avascular zone in diabetic retinopathy. *Graefe's Arch Clin Exp Ophthalmol* 2015; [Epub ahead of print].
56. Agemy SA, Scripsema NK, Shah CM *et al.* Retinal vascular perfusion density mapping using optical coherence tomography angiography in normals and diabetic retinopathy patients. *Retina* 2015; 35: 2353–2363.
57. Coscas GJ, Lupidi M, Coscas F, Cagini C & Souied EH. Optical coherence tomography angiography versus traditional multimodal imaging in assessing the activity of exudative age-related macular degeneration: a new diagnostic challenge. *Retina* 2015; 35: 2219–2228.
58. Moult E, Choi W, Waheed NK *et al.* Ultrahigh-speed swept-source OCT angiography in exudative AMD. *Ophthalmic Surg Lasers Imaging Retina* 2014; 45: 496–505.
59. Miere A, Querques G, Semoun O *et al.* Optical coherence tomography angiography in early type 3 neovascularization. *Retina* 2015; 35: 2236–2241.
60. Kuehlewein L, Dansingani KK, de Carlo TE *et al.* Optical coherence tomography angiography of type 3 neovascularization secondary to age-related macular degeneration. *Retina* 2015; 35: 2229–2235.
61. El Ameen A, Cohen SY, Semoun O *et al.* Type 2 neovascularization secondary to age-related macular degeneration imaged by optical coherence tomography angiography. *Retina* 2015; 35: 2212–2218.
62. Jia Y, Bailey ST, Wilson D *et al.* Quantitative optical coherence tomography angiography of choroidal neovascularization in age-related macular degeneration. *Ophthalmology* 2014; 121: 1435–1444.
63. Kuehlewein L, Bansal M, Lenis TL *et al.* Optical coherence tomography angiography of type 1 neovascularization in age-related macular degeneration. *Am J Ophthalmol* 2015; 160: 739–748 e2.
64. Dansingani KK & Freund KB. Optical coherence tomography angiography reveals mature, tangled vascular networks in eyes with neovascular age-related macular degeneration showing resistance to geographic atrophy. *Ophthalmic Surg Lasers Imaging Retina* 2015; 46: 907–912.
65. Muakkassa NW, Chin AT, de Carlo T *et al.* Characterizing the effect of anti-vascular endothelial growth factor therapy on treatment-naive choroidal neovascularization using optical coherence tomography angiography. *Retina* 2015; 35: 2252–2259.
66. Lumbroso B, Rispoli M & Savastano MC. Longitudinal optical coherence tomography-angiography study of type 2 naive choroidal neovascularization early response after treatment. *Retina* 2015; 35: 2242–2251.
67. Kuehlewein L, Sadda SR & Sarraf D. OCT angiography and sequential quantitative analysis of type 2 neovascularization after ranibizumab therapy. *Eye (Lond)* 2015; 29: 932–935.
68. Spaide RF. Optical coherence tomography angiography signs of vascular abnormalization with antiangiogenic therapy for choroidal neovascularization. *Am J Ophthalmol* 2015; 160: 6–16.
69. Coscas G, Lupidi M, Coscas F *et al.* Optical coherence tomography angiography during follow-up: qualitative and quantitative analysis of mixed type I and II choroidal neovascularization after vascular endothelial growth factor trap therapy. *Ophthalmic Res* 2015; 54: 57–63.
70. Huang D, Jia Y, Rispoli M, Tan O & Lumbroso B. Optical coherence tomography angiography of time course of chor-

oidal neovascularization in response to anti-angiogenic treatment. *Retina* 2015; 35: 2260–2264.
71. Miere A, Semoun O, Cohen SY *et al.* Optical coherence tomography angiography features of subretinal fibrosis in age-related macular degeneration. *Retina* 2015; 35: 2275–2284.
72. Zeimer M, Gutfleisch M, Heimes B *et al.* Association between changes in macular vasculature in optical coherence tomography- and fluorescein-angiography and distribution of macular pigment in type 2 idiopathic macular telangiectasia. *Retina* 2015; 35: 2307–2316.
73. Gaudric A, Krivosic V & Tadayoni R. Outer retina capillary invasion and ellipsoid zone loss in macular telangiectasia Type 2 imaged by optical coherence tomography angiography. *Retina* 2015; 35: 2300–2306.
74. Balaratnasingam C, Yannuzzi LA & Spaide RF. Possible choroidal neovascularization in macular telangiectasia type 2. *Retina* 2015; 35: 2317–2322.
75. Spaide RF, Klancnik JM Jr, Cooney MJ *et al.* Volume-rendering optical coherence tomography angiography of macular telangiectasia type 2. *Ophthalmology* 2015; 122: 2261–2269.
76. Zhang Q, Wang RK, Chen CL *et al.* Swept source optical coherence tomography angiography of neovascular macular telangiectasia type 2. *Retina* 2015; 35: 2285–2299.
77. Wang Q, Chan SY, Jonas JB & Wei WB. Optical coherence tomography angiography in idiopathic choroidal neovascularization. *Acta Ophthalmol* 2015; doi: 10.1111/aos.12841. [Epub ahead of print].
78. Klufas MA, O'Hearn T & Sarraf D. Optical coherence tomography angiography and widefield fundus autofluorescence in punctate inner choroidopathy. *Retin Cases Brief Rep* 2015; 9: 323–326.
79. Inoue M, Balaratnasingam C & Freund KB. Optical coherence tomography angiography of polypoidal choroidal vasculopathy and polypoidal choroidal neovascularization. *Retina* 2015; 35: 2265–2274.
80. Dansingani KK, Balaratnasingam C, Klufas MA, Sarraf D & Freund KB. Optical coherence tomography angiography of shallow irregular pigment epithelial detachments in pachychoroid spectrum disease. *Am J Ophthalmol* 2015; 160(6): 1243–1254.
81. Sanfilippo CJ, Klufas MA, Sarraf D & Tsui I. Optical coherence tomography angiography of sickle cell maculopathy. *Retin Cases Brief Rep* 2015; 9: 360–362.
82. Rispoli M, Savastano MC & Lumbroso B. Capillary network anomalies in branch retinal vein occlusion on optical coherence tomography angiography. *Retina* 2015; 35: 2332–2338.
83. Kashani AH, Lee SY, Moshfeghi A, Durbin MK & Puliafito CA. Optical coherence tomography angiography of retinal venous occlusion. *Retina* 2015; 35: 2323–2331.
84. Mastropasqua R, Di Antonio L, Di Staso S *et al.* Optical coherence tomography angiography in retinal vascular diseases and choroidal neovascularization. *J Ophthalmol* 2015; 2015: 343515.
85. Coscas F, Glacet-Bernard A, Miere A *et al.* Optical coherence tomography angiography in retinal vein occlusion: evaluation of superficial and deep capillary plexa. *Am J Ophthalmol* 2016; 161: 160–171.
86. Suzuki N, Hirano Y, Yoshida M *et al.* Microvascular abnormalities on optical coherence tomography angiography in macular edema associated with branch retinal vein occlusion. *Am J Ophthalmol* 2016 Jan; 161: 126–132.
87. Philippakis E, Dupas B, Bonnin P, Hage R, Gaudric A & Tadayoni R. Optical coherence tomography angiography shows deep capillary plexus hypoperfusion in incomplete central retinal artery occlusion. *Retin Cases Brief Rep* 2015; 9: 333–338.
88. Pecen PE, Smith AG & Ehlers JP. Optical coherence tomography angiography of acute macular neuroretinopathy and paracentral acute middle maculopathy. *JAMA Ophthalmol* 2015; 133(12): 1478–80.
89. Sridhar J, Shahlaee A, Rahimy E *et al.* Optical coherence tomography angiography and en face optical coherence tomography features of paracentral acute middle maculopathy. *Am J Ophthalmol* 2015; 160(6): 1259–1268.
90. Sharma P, Sridhar J, Rayess N & Maguire JI. Optical coherence tomography angiography (OCT-A) of type 2 retinal arteriovenous malformation. *Can J Ophthalmol* 2015; 50: e93–e96.
91. Veverka KK, AbouChehade JE, Iezzi R Jr & Pulido JS. Noninvasive grading of radiation retinopathy: the use of optical coherence tomography angiography. *Retina* 2015; 35: 2400–2410.
92. Spaide RF. Volume rendering of optical coherence tomography angiography reveals extensive retinal vascular contributions to neovascularization in ocular toxoplasmosis. *Retina* 2015; 35: 2421–2422.
93. Bonini Filho MA, de Carlo TE, Ferrara D *et al.* Association of choroidal neovascularization and central serous chorioretinopathy with optical coherence tomography angiography. *JAMA Ophthalmol* 2015; 133: 899–906.
94. de Carlo TE, Bonini Filho MA, Chin AT *et al.* Spectral-domain optical coherence tomography angiography of choroidal neovascularization. *Ophthalmology* 2015; 122: 1228–1238.
95. Teussink MM, Breukink MB, van Grinsven MJ *et al.* OCT angiography compared to fluorescein and indocyanine green angiography in chronic central serous chorioretinopathy. *Invest Ophthalmol Vis Sci* 2015; 56: 5229–5237.
96. de Carlo TE, Bonini Filho MA, Adhi M, Duker JS. Retinal and choroidal vasculature in birdshot chorioretinopathy analyzed using spectral domain optical coherence tomography angiography. *Retina* 2015; 35: 2392–2399.
97. Pechauer AD, Jia Y, Liu L *et al.* Optical coherence tomography angiography of peripapillary retinal blood flow

response to hyperoxia. *Invest Ophthalmol Vis Sci* 2015; 56: 3287–3291.
98. Wang X, Jia Y, Spain R *et al.* Optical coherence tomography angiography of optic nerve head and parafovea in multiple sclerosis. *Br J Ophthalmol* 2014; 98: 1368–1373.
99. Wang X, Jiang C, Ko T *et al.* Correlation between optic disc perfusion and glaucomatous severity in patients with open-angle glaucoma: an optical coherence tomography angiography study. *Graefe's Arch Clin Exp Ophthalmol* 2015; 253: 1557–1564.
100. Liu L, Jia Y, Takusagawa HL *et al.* Optical coherence tomography angiography of the peripapillary retina in glaucoma. *JAMA Ophthalmol* 2015; 133: 1045–1052.
101. Jia Y, Wei E, Wang X *et al.* Optical coherence tomography angiography of optic disc perfusion in glaucoma. *Ophthalmology* 2014; 121: 1322–1332.
102. Liu L, Gao SS, Bailey ST *et al.* Automated choroidal neovascularization detection algorithm for optical coherence tomography angiography. *Biomed Opt Express* 2015; 6: 3564–3576.
103. Spaide RF, Koizumi H & Pozzoni MC. Enhanced depth imaging spectral-domain optical coherence tomography. *Am J Ophthalmol* 2008; 146: 496–500.
104. Laviers H & Zambarakji H. Enhanced depth imaging-OCT of the choroid: a review of the current literature. *Graefe's Arch Clin Exp Ophthalmol* 2014; 252: 1871–1883.
105. Strouthidis NG, Fortune B, Yang H, Sigal IA & Burgoyne CF. Longitudinal change detected by spectral domain optical coherence tomography in the optic nerve head and peripapillary retina in experimental glaucoma. *Invest Ophthalmol Vis Sci* 2011; 52: 1206–1219.
106. Ren R, Yang H, Gardiner SK *et al.* Anterior lamina cribrosa surface depth, age, and visual field sensitivity in the Portland Progression Project. *Invest Ophthalmol Vis Sci* 2014; 55: 1531–1539.
107. Chauhan BC, O'Leary N, Almobarak FA *et al.* Enhanced detection of open-angle glaucoma with an anatomically accurate optical coherence tomography-derived neuroretinal rim parameter. *Ophthalmology* 2013; 120: 535–543Epub 2012/12/26.
108. Gardiner SK, Ren R, Yang H *et al.* A method to estimate the amount of neuroretinal rim tissue in glaucoma: comparison with current methods for measuring rim area. *Am J Ophthalmol* 2014;157:540–9 e1-2. Epub 2013/11/19.
109. Lujan BJ, Roorda A, Knighton RW & Carroll J. Revealing Henle's fiber layer using spectral domain optical coherence tomography. *Invest Ophthalmol Vis Sci* 2011; 52: 1486–1492Epub 2010/11/13.
110. Miller DT, Kocaoglu OP, Wang Q & Lee S. Adaptive optics and the eye (super resolution OCT). *Eye (Lond)* 2011; 25: 321–330. Epub 2011/03/11.
111. Pircher M & Zawadzki RJ. Combining adaptive optics with optical coherence tomography: unveiling the cellular structure of the human retina in vivo. *Expert Rev Ophthalmol* 2007; 2: 1019–1035.
112. Kocaoglu OP, Turner TL, Liu Z & Miller DT. Adaptive optics optical coherence tomography at 1 MHz. *Biomed Opt Express* 2014; 5: 4186–4200.
113. Felberer F, Kroisamer JS, Baumann B *et al.* Adaptive optics SLO/OCT for 3D imaging of human photoreceptors in vivo. *Biomed Opt Express* 2014; 5: 439–456.
114. Kocaoglu OP, Lee S, Jonnal RS *et al.* Imaging cone photoreceptors in three dimensions and in time using ultrahigh resolution optical coherence tomography with adaptive optics. *Biomed Opt Express* 2011; 2: 748–763.
115. Kocaoglu OP, Cense B, Jonnal RS *et al.* Imaging retinal nerve fiber bundles using optical coherence tomography with adaptive optics. *Vision Res* 2011; 51: 1835–1844.
116. Kim DY, Werner JS & Zawadzki RJ. Complex conjugate artifact-free adaptive optics optical coherence tomography of in vivo human optic nerve head. *J Biomed Opt* 2012; 17: 126005.
117. Nadler Z, Wang B, Schuman JS *et al.* In vivo three-dimensional characterization of the healthy human lamina cribrosa with adaptive optics spectral-domain optical coherence tomography. *Invest Ophthalmol Vis Sci* 2014; 55: 6459–6466.
118. Felberer F, Rechenmacher M, Haindl R *et al.* Imaging of retinal vasculature using adaptive optics SLO/OCT. *Biomed Opt Express* 2015; 6: 1407–1418.
119. Kurokawa K, Sasaki K, Makita S, Hong YJ & Yasuno Y. Three-dimensional retinal and choroidal capillary imaging by power Doppler optical coherence angiography with adaptive optics. *Opt Express* 2012; 20: 22796–22812.
120. Venkateswaran K, Roorda A & Romero-Borja F. Theoretical modeling and evaluation of the axial resolution of the adaptive optics scanning laser ophthalmoscope. *J Biomed Opt* 2004; 9: 132–138.
121. Song H, Chui TY, Zhong Z, Elsner AE & Burns SA. Variation of cone photoreceptor packing density with retinal eccentricity and age. *Invest Ophthalmol Vis Sci* 2011; 52: 7376–7384.
122. Park SP, Chung JK, Greenstein V, Tsang SH & Chang S. A study of factors affecting the human cone photoreceptor density measured by adaptive optics scanning laser ophthalmoscope. *Exp Eye Res* 2013; 108: 1–9.
123. Garrioch R, Langlo C, Dubis AM, Cooper RF, Dubra A & Carroll J. Repeatability of in vivo parafoveal cone density and spacing measurements. *Optom Vis Sci* 2012; 89: 632–643.
124. Godara P, Siebe C, Rha J, Michaelides M & Carroll J. Assessing the photoreceptor mosaic over drusen using adaptive optics and SD-OCT. *Ophthalmic Surg Lasers Imaging* 2010; 41(Suppl): S104–S108.
125. Boretsky A, Khan F, Burnett G *et al.* In vivo imaging of photoreceptor disruption associated with age-related mac-

ular degeneration: a pilot study. *Lasers Surg Med* 2012; 44: 603–610.
126. Zayit-Soudry S, Duncan JL, Syed R, Menghini M & Roorda AJ. Cone structure imaged with adaptive optics scanning laser ophthalmoscopy in eyes with nonneovascular age-related macular degeneration. *Invest Ophthalmol Vis Sci* 2013; 54: 7498–7509.
127. Mrejen S, Sato T, Curcio CA & Spaide RF. Assessing the cone photoreceptor mosaic in eyes with pseudodrusen and soft Drusen in vivo using adaptive optics imaging. *Ophthalmology* 2014; 121: 545–551.
128. Obata R & Yanagi Y. Quantitative analysis of cone photoreceptor distribution and its relationship with axial length, age, and early age-related macular degeneration. *PLoS One* 2014; 9: e91873.
129. Meadway A, Wang X, Curcio CA & Zhang Y. Microstructure of subretinal drusenoid deposits revealed by adaptive optics imaging. *Biomed Opt Express* 2014; 5: 713–727.
130. Zhang Y, Wang X, Rivero EB *et al.* Photoreceptor perturbation around subretinal drusenoid deposits as revealed by adaptive optics scanning laser ophthalmoscopy. *Am J Ophthalmol* 2014; 158: 584–596 e1.
131. Querques G, Kamami-Levy C, Blanco-Garavito R *et al.* Appearance of medium-large drusen and reticular pseudodrusen on adaptive optics in age-related macular degeneration. *Br J Ophthalmol* 2014; 98: 1522–1527.
132. Land ME, Cooper RF, Young J *et al.* Cone structure in subjects with known genetic relative risk for AMD. *Optom Vis Sci* 2014; 91: 939–949.
133. Querques G, Kamami-Levy C, Georges A *et al.* Adaptive optics imaging of foveal sparing in geographic atrophy secondary to age-related macular degeneration. *Retina* 2016; 36(2): 247–54.
134. Choi SS, Zawadzki RJ, Lim MC *et al.* Evidence of outer retinal changes in glaucoma patients as revealed by ultrahigh-resolution in vivo retinal imaging. *Br J Ophthalmol* 2011; 95: 131–141.
135. Lombardo M, Parravano M, Lombardo G *et al.* Adaptive optics imaging of parafoveal cones in type 1 diabetes. *Retina* 2014; 34: 546–557.
136. Tan W, Wright T, Rajendran D *et al.* Cone-photoreceptor density in adolescents with type 1 diabetes. *Invest Ophthalmol Vis Sci* 2015; 56: 6339–6343.
137. Duncan JL, Zhang Y, Gandhi J *et al.* High-resolution imaging with adaptive optics in patients with inherited retinal degeneration. *Invest Ophthalmol Vis Sci* 2007; 48: 3283–3291.
138. Tojo N, Nakamura T, Fuchizawa C, Oiwake T & Hayashi A. Adaptive optics fundus images of cone photoreceptors in the macula of patients with retinitis pigmentosa. *Clin Ophthalmol* 2013; 7: 203–210.
139. Pyo Park S, Hwan Hong I, Tsang SH & Chang S. Cellular imaging demonstrates genetic mosaicism in heterozygous carriers of an X-linked ciliopathy gene. *Eur J Hum Genet* 2013; 21: 1240–1248.
140. Makiyama Y, Ooto S, Hangai M *et al.* Macular cone abnormalities in retinitis pigmentosa with preserved central vision using adaptive optics scanning laser ophthalmoscopy. *PLoS One* 2013; 8: e79447.
141. Park SP, Lee W, Bae EJ *et al.* Early structural anomalies observed by high-resolution imaging in two related cases of autosomal-dominant retinitis pigmentosa. *Ophthalmic Surg Lasers Imaging Retina* 2014; 45: 469–473.
142. Menghini M, Lujan BJ, Zayit-Soudry S *et al.* Correlation of outer nuclear layer thickness with cone density values in patients with retinitis pigmentosa and healthy subjects. *Invest Ophthalmol Vis Sci* 2015; 56: 372–381.
143. Gale MJ, Feng S, Titus HE, Smith TB & Pennesi ME. Interpretation of flood-illuminated adaptive optics images in subjects with Retinitis Pigmentosa. *Adv Exp Med Biol* 2016; 854: 291–297.
144. Chen Y, Ratnam K, Sundquist SM *et al.* Cone photoreceptor abnormalities correlate with vision loss in patients with Stargardt disease. *Invest Ophthalmol Vis Sci* 2011; 52: 3281–3292.
145. Song H, Rossi EA, Latchney L *et al.* Cone and rod loss in Stargardt disease revealed by adaptive optics scanning light ophthalmoscopy. *JAMA Ophthalmol* 2015; 133: 1198–1203.
146. Syed R, Sundquist SM, Ratnam K *et al.* High-resolution images of retinal structure in patients with choroideremia. *Invest Ophthalmol Vis Sci* 2013; 54: 950–961.
147. Morgan JI, Han G, Klinman E *et al.* High-resolution adaptive optics retinal imaging of cellular structure in choroideremia. *Invest Ophthalmol Vis Sci* 2014; 55: 6381–6397.
148. Genead MA, Fishman GA, Rha J *et al.* Photoreceptor structure and function in patients with congenital achromatopsia. *Invest Ophthalmol Vis Sci* 2011; 52: 7298–7308.
149. Dubis AM, Cooper RF, Aboshiha J *et al.* Genotype-dependent variability in residual cone structure in achromatopsia: toward developing metrics for assessing cone health. *Invest Ophthalmol Vis Sci* 2014; 55: 7303–7311.
150. Abozaid MA, Langlo CS, Dubis AM *et al.* Reliability and repeatability of cone density measurements in patients with congenital achromatopsia. *Adv Exp Med Biol* 2016; 854: 277–283.
151. Massamba N, Querques G, Lamory B *et al.* In vivo evaluation of photoreceptor mosaic in type 2 idiopathic macular telangiectasia using adaptive optics. *Acta Ophthalmol* 2011; 89: e601–e603.
152. Ooto S, Hangai M, Takayama K *et al.* High-resolution photoreceptor imaging in idiopathic macular telangiectasia type 2 using adaptive optics scanning laser ophthalmoscopy. *Invest Ophthalmol Vis Sci* 2011; 52: 5541–5550.
153. Ooto S, Hangai M, Takayama K *et al.* Comparison of cone pathologic changes in idiopathic macular telangiectasia types 1 and 2 using adaptive optics scanning laser ophthalmoscopy. *Am J Ophthalmol* 2013; 155: 1045–1057 e4.
154. Jacob J, Krivosic V, Paques M, Tadayoni R & Gaudric A. Cone density loss on adaptive optics in early macular

telangiectasia type 2. *Retina* 2015; http://www.ncbi.nlm.nih.gov/pubmed/26418443. Epub 2015/09/30.
155. Ooto S, Hangai M, Sakamoto A *et al.* High-resolution imaging of resolved central serous chorioretinopathy using adaptive optics scanning laser ophthalmoscopy. *Ophthalmology*. 2010;117:1800-9, 9 e1-2.
156. Curcio CA, Sloan KR, Kalina RE & Hendrickson AE. Human photoreceptor topography. *J Comp Neurol* 1990; 292: 497–523.
157. Dubra A & Sulai Y. Reflective afocal broadband adaptive optics scanning ophthalmoscope. *Biomed Opt Express* 2011; 2: 1757–1768.
158. Dubra A, Sulai Y, Norris JL *et al.* Noninvasive imaging of the human rod photoreceptor mosaic using a confocal adaptive optics scanning ophthalmoscope. *Biomed Opt Express* 2011; 2: 1864–1876.
159. Doble N, Choi SS, Codona JL *et al.* In vivo imaging of the human rod photoreceptor mosaic. *Opt Lett* 2011; 36: 31–33.
160. Merino D, Duncan JL, Tiruveedhula P & Roorda A. Observation of cone and rod photoreceptors in normal subjects and patients using a new generation adaptive optics scanning laser ophthalmoscope. *Biomed Opt Express* 2011; 2: 2189–2201.
161. Cooper RF, Dubis AM, Pavaskar A *et al.* Spatial and temporal variation of rod photoreceptor reflectance in the human retina. *Biomed Opt Express* 2011; 2: 2577–2589.
162. Sulai YN & Dubra A. Adaptive optics scanning ophthalmoscopy with annular pupils. *Biomed Opt Express* 2012; 3: 1647–1661.
163. Carroll J, Choi SS & Williams DR. In vivo imaging of the photoreceptor mosaic of a rod monochromat. *Vision Res* 2008; 48: 2564–2568.
164. Godara P, Cooper RF, Sergouniotis PI *et al.* Assessing retinal structure in complete congenital stationary night blindness and Oguchi disease. *Am J Ophthalmol* 2012; 154: 987–1001 e1.
165. Hansen SO, Cooper RF, Dubra A, Carroll J & Weinberg DV. Selective cone photoreceptor injury in acute macular neuroretinopathy. *Retina* 2013; 33: 1650–1658.
166. Strauss O. The retinal pigment epithelium in visual function. *Physiol Rev* 2005; 85: 845–881.
167. Roorda A, Zhang Y & Duncan JL. High-resolution in vivo imaging of the RPE mosaic in eyes with retinal disease. *Invest Ophthalmol Vis Sci* 2007; 48: 2297–2303.
168. Wang Q, Tuten WS, Lujan BJ *et al.* Adaptive optics microperimetry and OCT images show preserved function and recovery of cone visibility in macular telangiectasia type 2 retinal lesions. *Invest Ophthalmol Vis Sci* 2015; 56: 778–786.
169. Morgan JIW, Dubra A, Wolfe R, Merigan WH & Williams DR. In vivo autofluorescence imaging of the human and macaque retinal pigment epithelial cell mosaic. *Invest Ophthalmol Vis Sci* 2009; 50: 1350–1359.
170. Scoles D, Sulai YN & Dubra A. In vivo dark-field imaging of the retinal pigment epithelium cell mosaic. *Biomed Opt Express* 2013; 4: 1710–1723.
171. Dubra A & Harvey Z. Registration of 2D images from fast scanning ophthalmic instruments. *Lect Notes Comput Sci* 2010; 6204: 60–71.
172. Martin JA & Roorda A. Direct and noninvasive assessment of parafoveal capillary leukocyte velocity. *Ophthalmology* 2005; 112: 2219–2224.
173. Zhong Z, Petrig BL, Qi X & Burns SA. In vivo measurement of erythrocyte velocity and retinal blood flow using adaptive optics scanning laser ophthalmoscopy. *Opt Express* 2008; 16: 12746–12756.
174. Tam J, Martin JA & Roorda A. Noninvasive visualization and analysis of parafoveal capillaries in humans. *Invest Ophthalmol Vis Sci* 2010; 51: 1691–1698.
175. Zhong Z, Song H, Chui TY, Petrig BL & Burns SA. Noninvasive measurements and analysis of blood velocity profiles in human retinal vessels. *Invest Ophthalmol Vis Sci* 2011; 52: 4151–4157.
176. Tam J & Roorda A. Speed quantification and tracking of moving objects in adaptive optics scanning laser ophthalmoscopy. *J Biomed Opt* 2011; 16: 036002.
177. Tam J, Dhamdhere KP, Tiruveedhula P *et al.* Disruption of the retinal parafoveal capillary network in type 2 diabetes before the onset of diabetic retinopathy. *Invest Ophthalmol Vis Sci* 2011; 52: 9257–9266.
178. Chui TY, Zhong Z, Song H & Burns SA. Foveal avascular zone and its relationship to foveal pit shape. *Optom Vis Sci* 2012; 89: 602–610.
179. Tam J, Dhamdhere KP, Tiruveedhula P *et al.* Subclinical capillary changes in non-proliferative diabetic retinopathy. *Optom Vis Sci* 2012; 89: E692–E703.
180. Arichika S, Uji A, Hangai M, Ooto S & Yoshimura N. Noninvasive and direct monitoring of erythrocyte aggregates in human retinal microvasculature using adaptive optics scanning laser ophthalmoscopy. *Invest Ophthalmol Vis Sci* 2013; 54: 4394–4402.
181. Arichika S, Uji A, Ooto S, Miyamoto K & Yoshimura N. Adaptive optics-assisted identification of preferential erythrocyte aggregate pathways in the human retinal microvasculature. *PLoS One* 2014; 9: e89679.
182. Burns SA, Elsner AE, Chui TY *et al.* In vivo adaptive optics microvascular imaging in diabetic patients without clinically severe diabetic retinopathy. *Biomed Opt Express* 2014; 5: 961–974.
183. Arichika S, Uji A, Murakami T *et al.* Retinal hemorheologic characterization of early-stage diabetic retinopathy using adaptive optics scanning laser ophthalmoscopy. *Invest Ophthalmol Vis Sci* 2014; 55: 8513–8522.
184. Chui TY, VanNasdale DA, Elsner AE & Burns SA. The association between the foveal avascular zone and retinal thickness. *Invest Ophthalmol Vis Sci* 2014; 55: 6870–6877.

185. Takayama K, Ooto S, Hangai M *et al.* High-resolution imaging of the retinal nerve fiber layer in normal eyes using adaptive optics scanning laser ophthalmoscopy. *PLoS One* 2012; 7: e33158.
186. Takayama K, Ooto S, Hangai M *et al.* High-resolution imaging of retinal nerve fiber bundles in glaucoma using adaptive optics scanning laser ophthalmoscopy. *Am J Ophthalmol* 2013; 155: 870–881.
187. Chen MF, Chui TY, Alhadeff P *et al.* Adaptive optics imaging of healthy and abnormal regions of retinal nerve fiber bundles of patients with glaucoma. *Invest Ophthalmol Vis Sci* 2015; 56: 674–681.
188. Hood DC, Chen MF, Lee D *et al.* Confocal adaptive optics imaging of peripapillary nerve fiber bundles: implications for glaucomatous damage seen on circumpapillary OCT scans. *Transl Vis Sci Technol* 2015; 4: 12.
189. Huang G, Luo T, Gast TJ *et al.* Imaging glaucomatous damage across the temporal raphe. *Invest Ophthalmol Vis Sci* 2015; 56: 3496–3504.
190. Ivers KM, Li C, Patel N *et al.* Reproducibility of measuring lamina cribrosa pore geometry in human and nonhuman primates with in vivo adaptive optics imaging. *Invest Ophthalmol Vis Sci* 2011; 52: 5473–5480.
191. Akagi T, Hangai M, Takayama K *et al.* In vivo imaging of lamina cribrosa pores by adaptive optics scanning laser ophthalmoscopy. *Invest Ophthalmol Vis Sci* 2012; 53: 4111–4119.
192. Sredar N, Ivers KM, Queener HM, Zouridakis G & Porter J. 3D modeling to characterize lamina cribrosa surface and pore geometries using in vivo images from normal and glaucomatous eyes. *Biomed Opt Express* 2013; 4: 1153–1165.
193. Gray DC, Merigan W, Wolfing JI *et al.* In vivo fluorescence imaging of primate retinal ganglion cells and retinal pigment epithelial cells. *Opt Express* 2006; 14: 7144–7158.
194. Pinhas A, Dubow M, Shah N *et al.* In vivo imaging of human retinal microvasculature using adaptive optics scanning light ophthalmoscope fluorescein angiography. *Biomed Opt Express* 2013; 4: 1305–1317.
195. Dubow M, Pinhas A, Shah N *et al.* Classification of human retinal microaneurysms using adaptive optics scanning light ophthalmoscope fluorescein angiography. *Invest Ophthalmol Vis Sci* 2014; 55: 1299–1309.
196. Chui TY, Dubow M, Pinhas A *et al.* Comparison of adaptive optics scanning light ophthalmoscopic fluorescein angiography and offset pinhole imaging. *Biomed Opt Express* 2014; 5: 1173–1189.
197. Pinhas A, Razeen M, Dubow M *et al.* Assessment of perfused foveal microvascular density and identification of nonperfused capillaries in healthy and vasculopathic eyes. *Invest Ophthalmol Vis Sci* 2014; 55: 8056–8066.
198. Pinhas A, Dubow M, Shah N *et al.* Fellow eye changes in patients with nonischemic central retinal vein occlusion: assessment of perfused foveal microvascular density and identification of nonperfused capillaries. *Retina* 2015; 35: 2028–2036Epub 2015/05/02.
199. Delori FC, Dorey CK, Staurenghi G *et al.* In vivo fluorescence of the ocular fundus exhibits retinal pigment epithelium lipofuscin characteristics. *Invest Ophthalmol Vis Sci* 1995; 36: 718–729.
200. Rossi EA, Rangel-Fonseca P, Parkins K *et al.* In vivo imaging of retinal pigment epithelium cells in age related macular degeneration. *Biomed Opt Express* 2013; 4: 2527–2539.
201. Rossi EA, Chung M, Dubra A *et al.* Imaging retinal mosaics in the living eye. *Eye (Lond)* 2011; 25: 301–308.
202. Rangel-Fonseca P, Gomez-Vieyra A, Malacara-Hernandez D *et al.* Automated segmentation of retinal pigment epithelium cells in fluorescence adaptive optics images. *J Opt Soc Am A Opt Image Sci Vis* 2013; 30: 2595–2604.
203. Morgan JIW, Hunter JJ, Masella B *et al.* Light-induced retinal changes observed using high-resolution autofluorescence imaging of the retinal pigment epithelium. *Invest Ophthalmol Vis Sci* 2008; 49: 3715–3729.
204. Morgan JIW, Hunter JJ, Merigan WH & Williams DR. The reduction of retinal autofluorescence caused by light exposure. *Invest Ophthalmol Vis Sci* 2009; 50: 6015–6022.
205. Hunter JJ, Morgan JI, Merigan WH *et al.* The susceptibility of the retina to photochemical damage from visible light. *Prog Retin Eye Res* 2012; 31: 28–42.
206. ANSI. *American National Standard for Safe Use of Lasers ANSI Z136.1-2014*: Laser Institute of America; 2014.
207. Chui TY, Vannasdale DA & Burns SA. The use of forward scatter to improve retinal vascular imaging with an adaptive optics scanning laser ophthalmoscope. *Biomed Opt Express* 2012; 3: 2537–2549.
208. Chui TY, Gast TJ & Burns SA. Imaging of vascular wall fine structure in the human retina using adaptive optics scanning laser ophthalmoscopy. *Invest Ophthalmol Vis Sci* 2013; 54: 7115–7124.
209. Scoles D, Sulai YN, Langlo CS *et al.* In vivo imaging of human cone photoreceptor inner segments. *Invest Ophthalmol Vis Sci* 2014; 55: 4244–4251.
210. Burke TR, Duncker T, Woods RL *et al.* Quantitative fundus autofluorescence in recessive Stargardt disease. *Invest Ophthalmol Vis Sci* 2014; 55: 2841–2852.
211. Sulai YN, Scoles D, Harvey Z & Dubra A. Visualization of retinal vascular structure and perfusion with a nonconfocal adaptive optics scanning light ophthalmoscope. *J Opt Soc Am A Opt Image Sci Vis* 2014; 31: 569–579.
212. Talcott KE, Ratnam K, Sundquist SM *et al.* Longitudinal study of cone photoreceptors during retinal degeneration and in response to ciliary neurotrophic factor treatment. *Invest Ophthalmol Vis Sci* 2011; 52: 2219–2226.
213. Birch DG, Weleber RG, Duncan JL, Jaffe GJ & Tao W. Randomized trial of ciliary neurotrophic factor delivered by encapsulated cell intraocular implants for retinitis pigmentosa. *Am J Ophthalmol* 2013; 156: 283–292 e1.

214. FDA Cellular T & Gene Therapies Advisory Committee. *Cellular and Gene Therapies for Retinal Disorders*. June 29, 2011. pp. 14.
215. Hofer H, Singer B & Williams DR. Different sensations from cones with the same photopigment. *J Vis* 2005; 5: 444–454.
216. Rossi EA & Roorda A. The relationship between visual resolution and cone spacing in the human fovea. *Nat Neurosci* 2010; 13: 156–157.
217. Harmening WM, Tuten WS, Roorda A & Sincich LC. Mapping the perceptual grain of the human retina. *J Neurosci* 2014; 34: 5667–5677.
218. Bruce KS, Harmening WM, Langston BR *et al.* Normal perceptual sensitivity arising from weakly reflective cone photoreceptors. *Invest Ophthalmol Vis Sci* 2015; 56: 4431–4438.
219. Makous W, Carroll J, Wolfing JI *et al.* Retinal microscotomas revealed with adaptive-optics microflashes. *Invest Ophthalmol Vis Sci* 2006; 47: 4160–4167.
220. Yao XC, Yamauchi A, Perry B & George JS. Rapid optical coherence tomography and recording functional scattering changes from activated frog retina. *Appl Opt* 2005; 44: 2019–2023.
221. Bizheva K, Pflug R, Hermann B *et al.* Optophysiology: depth-resolved probing of retinal physiology with functional ultrahigh-resolution optical coherence tomography. *Proc Natl Acad Sci U S A* 2006; 103: 5066–5071.
222. Srinivasan VJ, Wojtkowski M, Fujimoto JG & Duker JS. In vivo measurement of retinal physiology with high-speed ultrahigh-resolution optical coherence tomography. *Opt Lett* 2006; 31: 2308–2310.
223. Srinivasan VJ, Chen Y, Duker JS & Fujimoto JG. In vivo functional imaging of intrinsic scattering changes in the human retina with high-speed ultrahigh resolution OCT. *Opt Express* 2009; 17: 3861–3877.
224. Jonnal RS, Rha J, Zhang Y *et al.* In vivo functional imaging of human cone photoreceptors. *Opt Express* 2007; 15: 16141–16160.
225. Grieve K & Roorda A. Intrinsic signals from human cone photoreceptors. *Invest Ophthalmol Vis Sci* 2008; 49: 713–719.
226. Rha J, Schroeder B, Godara P & Carroll J. Variable optical activation of human cone photoreceptors visualized using a short coherence light source. *Opt Lett* 2009; 34: 3782–3784.
227. Jonnal RS, Besecker JR, Derby JC *et al.* Imaging outer segment renewal in living human cone photoreceptors. *Opt Express* 2010; 18: 5257–5270.
228. Zhong Z, Huang G, Chui TY, Petrig BL & Burns SA. Local flicker stimulation evokes local retinal blood velocity changes. *J Vis* 2012; 12: 3.
229. Wei E, Jia Y, Tan O *et al.* Parafoveal retinal vascular response to pattern visual stimulation assessed with OCT angiography. *PLoS One* 2013; 8: e81343.

Jessica I. W. Morgan completed her Ph.D. in 2008 in Optical Engineering at the University of Rochester, where she developed the first protocol for imaging individual retinal pigment epithelial cells in the living retina by combining autofluorescence imaging with high-resolution adaptive optics scanning laser/light ophthalmoscopy and novel image processing techniques. Following her doctoral work, Dr. Morgan took a postdoctoral position at the University of Pennsylvania, where she developed protocols for measuring and quantifying rhodopsin in the living retina, to objectively assess visual cycle function. Currently, Dr. Morgan is an Assistant Professor of Ophthalmology at the Scheie Eye Institute in the Perelman School of Medicine at the University of Pennsylvania. Her current research focuses on investigating the pathogenesis of retinal disease through high-resolution retinal imaging, studying retinal structure and function on the cellular level longitudinally, and testing the safety and efficacy of experimental treatments for blinding disease.